

Gravitational-wave modes from precessing black-hole binaries

Michael Boyle,¹ Lawrence E. Kidder,¹ Serguei Ossokine,^{2,3} and Harald P. Pfeiffer^{2,4}

¹*Center for Radiophysics and Space Research, Cornell University, Ithaca, New York 14853, USA*

²*Canadian Institute for Theoretical Astrophysics, University of Toronto, 60 Saint George Street, Toronto, Ontario M5S 3H8, Canada*

³*Department of Astronomy and Astrophysics, 50 St. George Street, University of Toronto, Toronto, ON M5S 3H4, Canada*

⁴*Canadian Institute for Advanced Research, 180 Dundas St. West, Toronto, ON M5G 1Z8, Canada*

(Dated: September 24, 2014)

Gravitational waves from precessing black-hole binaries exhibit features that are absent in nonprecessing systems. The most prominent of these is a parity-violating asymmetry that beams energy and linear momentum preferentially along or opposite to the orbital angular momentum, leading to recoil of the binary. The asymmetry will appear as amplitude and phase modulations at the orbital frequency. For strongly precessing systems, it accounts for at least 3% amplitude modulation for binaries in the sensitivity band of ground-based gravitational-wave detectors, and can exceed 50% for massive systems. Such asymmetric features are also clearly visible when the waves are decomposed into modes of spin-weighted spherical harmonics, and are inherent in the waves themselves—rather than resulting from residual eccentricity in numerical simulations or from mode-mixing due to precession. In particular, there is generically no instantaneous frame for which the mode decomposition will have any symmetry. We introduce a method to simplify the expressions for waveforms given in analytical relativity, which can be used to combine existing high-order waveforms for nonprecessing systems with expressions for the precessing contributions, leading to improved accuracy and a unified treatment of precessing and nonprecessing binaries. Using this method, it is possible to clarify the nature and the origins of the asymmetries and show the effects of asymmetry on recoils more clearly. We present post-Newtonian (PN) expressions for the waveform modes that include these terms, complete to the relative 2PN level in spin (proportional to v^4/c^4 times a certain combination of the spins). Comparing the results of those expressions to numerical results, we find good qualitative agreement. We also demonstrate how these expressions can be used to efficiently calculate waveforms for gravitational-wave astronomy.

I. INTRODUCTION

The era of advanced gravitational-wave detectors will most likely bring dozens to hundreds of detections of black-hole binaries per year [1]. This raises the prospect of true gravitational-wave astronomy, with which we will be able to explore otherwise obscure regions of our universe. But the power of such exploration is limited by our ability to model the expected signals. Unless we can accurately model the gravitational waves emitted by a known or potential astrophysical source, we cannot know how sensitive our detection pipeline is to that type of source. Without understanding how physical characteristics are imprinted onto a waveform, we cannot expect to accurately measure any such characteristic or even know the accuracy of an attempted measurement—which diminishes the value of these detections to science. While simple approximate waveforms may be sufficient for initial detections and explorations of data-analysis techniques, gravitational-wave astronomy will require accurate waveforms [2–4].

Precessing black-hole binaries form a particularly interesting class of sources. These are systems in which one or both black holes have spin misaligned with the orbital axis, causing motion of that axis as the binary evolves. Precession encodes a wealth of information in the gravitational-wave signal, which can break degeneracies and allow the unambiguous measurement of various features of the source [5]. Though the uncertainties are great, these systems likely constitute a significant portion of potential black-hole binaries to which advanced detectors will be sensitive [6–11]. Unfortunately, the richness of these signals entails added complexity in the corresponding models.

Nonprecessing systems exhibit various symmetries, which reduce the complexity of the systems. For example, the black-hole spins are essentially constant,¹ and two of the three orbital rotational degrees of freedom are eliminated. Moreover, essentially all quantities will be smoothly monotonic and will vary on the inspiral timescale. Precessing systems, on the other hand, break all symmetries. The spins rotate, and all three degrees of orbital rotational freedom are engaged. More importantly, essentially all quantities vary on orbital timescales. Even in their simplest forms, the dominant components of the gravitational waves—which are usually quite smooth, monotonic, and symmetric—oscillate asymmetrically, as seen in Fig. 1.

While modern numerical codes can simulate precessing black-hole binaries robustly, the results are meaningless accumulations of numbers unless we can relate them to analytical models [16]. But this task is made far more challenging by the lack of symmetry. Our purpose here is to explore some of the features unique to precessing systems, and show that the problem can be made tractable by representing the data in appropriate ways. We will introduce new ways of measuring waveforms and a new way of expressing analytical models. In so doing, we will find that analytical models can be efficient both conceptually and computationally, while accurately reproducing the key features of precessing waveforms.

¹ The spin directions should be precisely constant, while the spin magnitudes will experience a gradual (2PN) change [12].

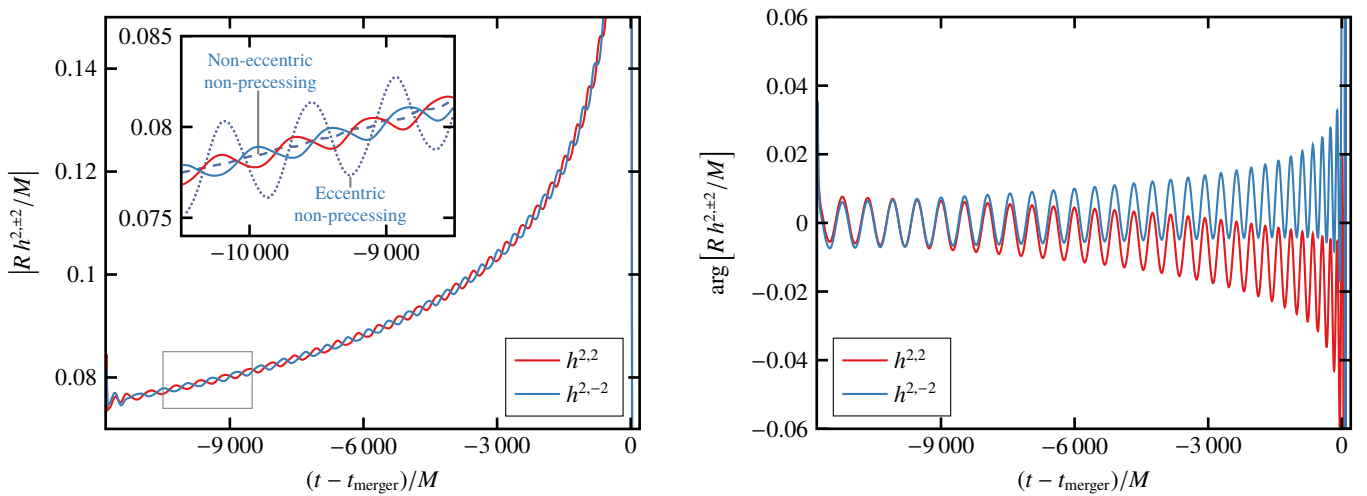


FIG. 1. **Dominant modes of a precessing system.** These plots show the amplitudes (left) and phases (right) of the $h^{2,\pm 2}$ modes from a numerical evolution of an equal-mass binary black-hole system with an initial spin of $\chi = 0.5$ in the orbital plane on one hole, and no spin on the other. For comparison, the inset of the left panel also show the curves for equal-mass nonspinning systems with very low eccentricity (dashed curve) and eccentricity $e \approx 0.02$ (dotted curve); the $h^{2,2}$ modes are plotted, but are identical to the $h^{2,-2}$ modes for these nonprecessing systems. In all cases, the data are extrapolated to infinite radius [13, 14] and are measured in the co-rotating frame [15], meaning that as much time dependence as possible has been removed from the waveform by a rotation of the coordinate system. The amplitude plot shows that the two modes of the precessing system alternate in dominance: when the $(\ell, m) = (2, 2)$ mode dominates, more power is beamed above the orbital plane (along the angular velocity); when the $(2, -2)$ mode dominates, more power is beamed below the orbital plane (opposite to the angular velocity). The period of this oscillation is very nearly equal to the orbital period. Similar features can be seen in other modes. Notably, the period of oscillation is roughly independent of the m value; it is always close to the orbital period. The phase plot exhibits oscillations on the same timescale. Because these oscillations are in phase with each other, it is clear that they could not be simultaneously eliminated from both modes—at least with a rotation about the Z axis of the decomposition frame. For example, if we were to transform to a frame in which the phase of the $h^{2,2}$ mode were constant, the oscillations in the phase of the $h^{2,-2}$ mode would be roughly twice as large. The nonprecessing systems shown in the inset of the plot on the left would appear on this plot as very nearly constant curves close to 0.

To begin, we combine the usual components of the transverse-traceless projection of the metric perturbation² at time t and location \vec{r} relative to the binary, $h_+(t, \vec{r})$ and $h_\times(t, \vec{r})$, into a single complex quantity $h(t, \vec{r}) := h_+(t, \vec{r}) - i h_\times(t, \vec{r})$. At each instant of time, h is measured on a coordinate sphere, and we abuse notation slightly by discussing $h(t, \hat{r})$ while suppressing the radius of the sphere.³ Finally, we decompose the angular dependence as an expansion in spin-weighted spherical harmonics (SWSHs) [17–19] so that

$$h(t, \hat{r}) = \sum_{\ell, m} h^{\ell, m}(t) {}_{-2}Y_{\ell, m}(\hat{r}). \quad (1)$$

Thus, we generally discuss the modes $h^{\ell, m}(t)$, rather than the function value in any particular direction. This representation has the advantage of transforming simply under rotations—a crucial feature when dealing with precessing systems. In particular, if $\hat{h}^{\ell, m}$ are the modes measured in a second coordinate

system—for instance, one that is adapted to the instantaneous orbital plane—then we have

$$\hat{h}^{\ell, m} = \sum_{m'} h^{\ell, m'} \mathfrak{D}_{m', m}^{(\ell)}(R^{-1}), \quad (2)$$

where $\mathfrak{D}^{(\ell)}$ is the usual Wigner matrix and R rotates the first set of basis vectors into the second. We show in Appendix B that the value of the field can be efficiently calculated from the modes in the rotating coordinate system, without first going through the numerically expensive transformation of Eq. (2)—which leads us to suggest that this may also be a useful representation of the waveform in data analysis for gravitational-wave detectors.

One of the more familiar expressions for the modes in nonprecessing binaries expresses the invariance of the system under reflection across the orbital plane (generally taken to coincide with the x - y plane):⁴

$$h^{\ell, m} = (-1)^{\ell} \bar{h}^{\ell, -m}. \quad (3)$$

This relationship obviates the need to separately analyze modes with negative values of m , for example. In particular, this means

² The methods and conclusions of this paper are essentially unchanged when considering the Newman–Penrose quantity Ψ_4 in place of h . For simplicity, we will only discuss h explicitly.

³ In fact, notation is frequently abused further by using h to represent the leading-order behavior of $|\vec{r}|h$ as the radius of the sphere approaches infinity.

⁴ This equation is derived and discussed in greater detail in Appendix C.

that the complex amplitudes of the two modes ($\ell, \pm m$) are equal, and their complex phases are opposite (up to an addition of π for odd ℓ). Equation (3) and its related properties are, of course, not true of nonprecessing binaries when the orbital plane does not coincide with the x - y plane of the coordinate system used to decompose the SWSHs, and is generally not true for precessing binaries in any coordinate system—as exemplified in Fig. 1. Similarly, a common expression for the dependence of the modes on orbital phase Φ is⁵

$$h^{\ell,m} \propto e^{-im\Phi}. \quad (4)$$

Again, this is incorrect even for nonprecessing binaries if the orbital plane and the x - y plane do not coincide, and generally not true for precessing binaries in any coordinate system.

The crucial fact in the failures of Eqs. (3) and (4) for precessing binaries, however, is that those equations are not incorrect just because of mode mixing as the orbital plane precesses while the decomposition basis is left fixed. Even if we allow rotations of the decomposition frame used to measure the waveform modes, we will see that there is no frame in which these equations would be true. Instead, even in the simplest frame, both Eqs. (3) and (4) are wrong for precessing systems at the 1PN level (proportional to v^2 times a certain combination of the spins). Since $v \gtrsim 0.1$ for essentially all black-hole binary systems expected to be visible to advanced gravitational-wave detectors, these discrepancies can have relative magnitudes of $v^2 \gtrsim 1\%$, depending on the spin, even at the lowest frequencies to which the detectors are sensitive—and they constitute ever-increasing proportions of the signal as the system inspirals. We will also find terms contributing to $h^{\ell,m}$ for precessing systems that are proportional to $e^{-i(m\pm 1)\Phi}$; because of these factors, the 1PN amplitude effects will oscillate on orbital timescales.

Several techniques have been introduced to simplify waveform modes by rotating the frame with respect to which the modes are decomposed. Whereas the waveforms may originally be decomposed with respect to a static basis ($\hat{x}, \hat{y}, \hat{z}$), a new frame is defined by constructing another basis ($\hat{X}, \hat{Y}, \hat{Z}$) at each moment in time, and expressing the modes $h^{\ell,m}$ with respect to this dynamic basis. We might distinguish two such types of frame determined by the waveforms themselves. First is the co-precessing frame [20–22], in which the waveform is still rotating; the \hat{Z} axis is aligned with a certain feature in the waveform, but the rotation of that frame is otherwise minimized. Second is the co-rotating frame [15], in which the waveform is not rotating at all. Both of these frames can be determined from the waveforms alone.

There are also two closely analogous frames that can be useful for PN systems. These are defined with respect to the

binary’s orbital elements—the positions and velocities of the black holes—rather than the waveforms. First is a frame we might call the “co-nutating” frame (for reasons that will become clear in Sec. II C), in which the \hat{Z} axis is aligned with the orbital angular velocity, but the rotation of that frame is otherwise minimized. This frame was introduced in Ref. [23] with an eye toward simplifying the analysis of gravitational-wave data from detectors. Here, we are concerned exclusively with constructing simple, accurate models of gravitational waves. We therefore introduce a final frame: the “co-orbital” frame, in which the binary itself is not moving at all. We discuss this further in Sec. III A.

Decomposing waveform modes in any of these four frames will indeed simplify certain features. However, the key point is that while a rotation can introduce parity-violating asymmetries where there would otherwise be none, no rotation can eliminate asymmetries in waveforms from precessing systems, as we will show in Sec. II B. Moreover, the asymmetries fluctuate on an orbital timescale. Thus, *accurate precessing waveforms must always have features varying on the orbital timescale*, regardless of the decomposition frame.

Fortunately, these features arise from terms that already appear in the PN literature [24–29], though in somewhat obscure form and with little direct discussion of their effects. In this paper, we will use recent advances in the treatment of waveforms from precessing systems to discuss these features in detail, clarify their origins, and correct some misconceptions that seem to have arisen in the literature. We exhibit the relevant PN expressions for these effects in terms of the $h^{\ell,m}$ modes using a simple and unified framework, at the highest order currently available, so that they may be easily incorporated into future work requiring accurate waveform models.

We begin in Sec. II by simply demonstrating several manifestations of the asymmetries in numerical data—first, in a familiar but potentially ambiguous way; then, in various geometrically unambiguous ways. In particular, we introduce rotationally invariant measures of asymmetry and parity violation. In Sec. III, we introduce the co-orbital frame more precisely. We use the co-orbital frame to express the PN waveforms for precessing systems, and to understand the origin of the asymmetric features. We then demonstrate that the same features seen in the numerical data are also present in post-Newtonian waveforms when these terms are included. The impact on binary recoil is briefly discussed in Sec. IV, where the effects of parity violation on the recoil are analyzed in detail. Finally, we summarize the discussion in Sec. V. Three appendices are also included. The first gives explicit formulas for the contributions to the PN waveform from terms involving spin, which allow for immediate implementation. The second appendix exhibits an efficient method for evaluating the waveform an inertial observer would measure, given a waveform in a rotating frame—by means of which we can avoid ~ 1000 evaluations of elements of the Wigner $\mathfrak{D}^{(\ell)}$ matrices at each time step, while improving the accuracy of the result. The final appendix discusses various details of antisymmetry and parity violation necessary for deriving results used in Sec. II B.

⁵ It must be noted that this expression gives the dependence of $h^{\ell,m}$ on the orbital phase for nonprecessing systems, but is sometimes incorrectly understood to also give the behavior of the complex phase of $h^{\ell,m}$. That is wrong even for nonprecessing systems at the 2.5PN level, because the proportionality is given by a time-dependent complex factor.

Explicit implementations of all the methods and results of this paper are also provided as computer code included among the [ancillary files](#) on this paper’s arXiv page.

II. ASYMMETRIES IN NUMERICAL DATA

We begin our discussion of the asymmetries by exhibiting them in data from a numerical evolution of a representative precessing binary; comparable features are found in other precessing systems. We choose a system in which one black hole is nonspinning and the other has a dimensionless spin of $\chi = 0.5$, initially in the orbital plane.⁶ The masses are nearly equal, with a relative mass difference $(M_1 - M_2)/(M_1 + M_2) \approx 0.02$, where M_1 and M_2 are the component masses. The orbital eccentricity of this numerical simulation is estimated to be $e \approx 3 \times 10^{-4}$. Oscillations in phase and amplitude due to orbital eccentricity for this system are proportional to e [31], and are much smaller for this system than the features visible in Fig. 1.

We demonstrate several different aspects of the asymmetry. First, we discuss asymmetries in the context of the waveform as decomposed into spin-weighted spherical-harmonic (SWSH) modes. Though this is perhaps the most familiar representation of gravitational waveforms, there may be some concern, in that individual modes are not rotationally invariant, and therefore do not provide a robust measure of asymmetry. We therefore introduce rotationally invariant integrals of the waveform—expressed as combinations of the modes—that unambiguously describe the asymmetries. Finally, we will examine various quantities describing the geometry and dynamics of the waveform and of the binary itself.

A. Waveform modes

Figure 1 shows the amplitudes (left panel) and phases (right panel) of the $h^{2,\pm 2}$ modes of the waveform. These quantities are measured in the co-rotating frame [15], in which as much of the time dependence as possible is absorbed into a time-dependent rotation. Both plots show oscillations on the orbital timescale, and substantial differences between the $h^{2,2}$ and $h^{2,-2}$ modes. A nonprecessing system would have very smooth curves with no apparent features on the orbital timescale and the amplitudes of the two modes would be identical. Furthermore, for such a nonprecessing binary represented in the co-rotating frame, the usual increases of the phase by multiples of 2π per orbit are absent. Any remaining variations of the phases would appear oppositely in the $h^{2,2}$ and $h^{2,-2}$ modes, in accordance with Eq. (3) but in contrast to what is observed in Fig. 1. However, the features we see in the precessing system are *not* artifacts of the attitude; we will see in Sec. II B that they cannot be eliminated through rotation of the decomposition basis.

Because of the structure of the SWSHs, the ${}_{-2}Y_{\ell,m}$ with positive m values have greater amplitude in directions with

positive z values; harmonics with negative m values have greater amplitude in directions with negative z values. (This is in contrast with the more familiar scalar spherical harmonics, and is required for compatibility between the behavior of spin-weighted functions and the naive tangent basis defined with respect to spherical coordinates.) As a result, whenever $|h^{2,2}| > |h^{2,-2}|$, net energy and linear momentum are beamed *along* the orbital angular velocity; when $|h^{2,2}| < |h^{2,-2}|$, more the net momenta are beamed *opposite* the angular velocity.

As shown by the formulas in Appendix A, when the orbital plane coincides with the x - y plane, the relative amplitude difference between the $(2, \pm 2)$ modes is given at lowest order in PN theory as

$$\frac{|h^{2,2}| - |h^{2,-2}|}{|h^{2,2}| + |h^{2,-2}|} \approx -v^2 \frac{\vec{\Sigma} \cdot \hat{\lambda}}{2M^2}. \quad (5)$$

Here, $\vec{\Sigma}/M = M_2 \vec{\chi}_2 - M_1 \vec{\chi}_1$, with $\vec{\chi}_1$ and $\vec{\chi}_2$ being the dimensionless spins of the two black holes; M is the sum of the two component masses; v is the standard PN-expansion parameter—roughly the relative speed of the black holes; and $\hat{\lambda}$ is a unit vector in the orbital plane, orthogonal to the black-hole separation vector.

Because Σ/M^2 can be of order unity, the asymmetry between $h^{2,2}$ and $h^{2,-2}$ will be substantial in the late stages of a binary black hole inspiral, where the velocity approaches $v \approx 1$. Even at the 10 Hz low-frequency “seismic wall” of advanced earthbound gravitational-wave detectors [32, 33], for the very low total mass of $10 M_\odot$ the relative amplitude difference given by Eq. (5) is 0.7 % in strongly precessing systems. Furthermore, the size of this effect will only grow as the system approaches merger, exceeding 3 % at the frequencies to which advanced LIGO will be most sensitive. Higher-mass systems will exhibit correspondingly larger oscillations at the same frequencies. Generally, we can expect any system to have relative asymmetries of as much as 8 % at the innermost stable circular orbit (ISCO) [34], which is generally taken as the point at which PN approximations break down. The numerical data for the system shown here reach relative differences of 14 % just after merger. Extrapolating with the scaling from PN theory, this suggests that strongly precessing systems could exhibit differences greater than 50 %.

Though the $h^{2,\pm 2}$ modes shown here exhibit the largest oscillations and asymmetries in an absolute sense, higher harmonics exhibit larger effects relative to their overall amplitudes. Generally, we can conclude that precessing systems exhibit strong amplitude and phase modulations throughout their evolution. These features must be modeled if we wish to obtain accurate waveforms and extract accurate physics.

B. Rotationally invariant measures of asymmetry

The complicated transformation law of Eq. (2) suggests that we cannot expect the relative amplitude difference given in Eq. (5) to be rotationally invariant. For example, we could flip the sign of the left-hand side of Eq. (5) by rotating \hat{z} into $-\hat{z}$. It is natural to wonder if we could remove the asymmetries

⁶ Specifically, this is run `SXS:BBH:0003` described in Ref. [30].

entirely simply by rotating the system. Here, we introduce two rotationally invariant measures of the asymmetry; because of their invariance and the fact that they are nonzero for precessing systems, this demonstrates that no rotation can remove the asymmetry.

There are two important qualities of the asymmetry shown in Fig. 1. First, is the simple fact that the magnitude of the waveform in one direction is different from the magnitude in the opposite direction—its antipode. We introduce the antipodal operator A , which transforms a field into that field evaluated at the antipodes. Let $f(\hat{r})$ be a function defined on the unit sphere (e.g., a SWSH). For any direction \hat{r} , we define

$$A\{f\}(\hat{r}) := f(-\hat{r}). \quad (6)$$

We will, of course, be most interested in fields of spin weight $s = -2$. As shown in Appendix C, A reverses the spin weight of such fields. To ensure that our results behave properly under rotations, we must reverse the spin weight again by taking the complex conjugate of the field. In particular, we define the *conjugate* antipodal operator

$$\bar{A}\{f\}(\hat{r}) := \bar{f}(-\hat{r}). \quad (7)$$

We can now apply this to the particular case of $f = h$. We drop the time dependence of h , stipulating that the following formulas apply separately at each instant of time. The effect of \bar{A} on the waveform modes is calculated in Appendix C, giving the fairly simple relation

$$\bar{A}\{h\}^{\ell,m} = (-1)^{\ell+m} \bar{h}^{\ell,-m}. \quad (8)$$

We define the projection operator $\Pi_{\bar{A}} := \frac{1}{2}(1 - \bar{A})$, which leaves only the antisymmetric part of the waveform. Using the involution property $\bar{A}^2 = 1$, it is trivial to compute that $\Pi_{\bar{A}}\{h\}$ is an eigenfunction of \bar{A} with eigenvalue -1 ; that is, we have succeeded in extracting that part of the waveform that reverses sign under \bar{A} . We then use this projection to define the normalized antisymmetry

$$a := \sqrt{\frac{\int |\Pi_{\bar{A}}\{h\}|^2 d\Omega}{\int |h|^2 d\Omega}} \quad (9a)$$

$$= \sqrt{\frac{\sum_{\ell,m} |h^{\ell,m} - (-1)^{\ell+m} \bar{h}^{\ell,-m}|^2}{4 \sum_{\ell,m} |h^{\ell,m}|^2}}. \quad (9b)$$

Though it is less familiar than the $h^{2,\pm 2}$ modes seen above, this quantity has the advantages of being rotationally invariant⁷ and

⁷ To understand the behavior of h and $A\{h\}$ under rotations, it is sufficient to consider the value of the fields measured at \hat{r} and $-\hat{r}$ when the rotation is about that axis. For spin-weighted fields, the rotation will induce opposite phase rotations, whereas we need the phases to vary in the *same* way if their difference is to be independent of attitude. This is why we need to use the complex conjugate in defining $\Pi_{\bar{A}}$. It is also easy to use the transformation law (2) and various properties of the $\mathcal{D}^{(\ell)}$ matrices to show explicitly that the particular combination of modes seen in Eq. (9b) is independent of the rotation operator R . The proof is given in the [ancillary files](#).

incorporating information about the complete function, rather than just a few select modes. This antisymmetry is also related to the binary recoil due to emission of linear momentum in the form of gravitational waves, as discussed further in Sec. IV.

The antisymmetry a can be nonzero in nonprecessing systems if the masses or spins of the black holes are unequal [25, 35–37]. The second quality of asymmetry we wish to discuss is one that is found only in precessing systems: inherent parity violation. In particular, a nonprecessing system will be symmetric under reflection through the x - y plane. This “ z -parity” operation is distinct from the closely related standard parity operation in three-dimensional physics, which reverses the sign of all spatial vector components; the two are related by an additional rotation through π about the z axis. Taking into account the spin weight, Appendix C shows that the effect of the z -parity operator P_z on h is

$$P_z\{h\}(\hat{r}) = \bar{h}(P_z\{\hat{r}\}). \quad (10)$$

Again, we can find a simple expression in terms of the effect on the waveform modes:

$$P_z\{h\}^{\ell,m} = (-1)^\ell \bar{h}^{\ell,-m}. \quad (11)$$

[This shows that Eq. (3) is just the statement that $h = P_z\{h\}$ for nonprecessing systems when the orbital plane is orthogonal to \hat{z} .] And again, we construct a projection operator $\Pi_z := \frac{1}{2}(1 - P_z)$, which leaves only the part of the waveform that is antisymmetric under P_z . Unfortunately, the result of this operator does not behave well under rotations—note the crucial factor of $(-1)^m$ in Eq. (8). This is a natural consequence of the special choice of z axis in the definition of P_z , and presents an obstacle to defining a rotationally invariant measure of parity violation analogous to the antisymmetry a . It is worth recalling that our intention is to show that this parity violation is present in any frame used to measure the waveform. We can achieve that goal and ensure rotational invariance by defining the normalized parity violation as the *minimum* such value, over all possible attitudes \mathcal{R} :⁸

$$p_{\min} := \min_{\mathcal{R}} \sqrt{\frac{\int |\Pi_z\{\mathcal{R}\{h\}\}|^2 d\Omega}{\int |\mathcal{R}\{h\}|^2 d\Omega}} \quad (12a)$$

$$= \min_{\mathcal{R}} \sqrt{\frac{\sum_{\ell,m} |\mathcal{R}\{h\}^{\ell,m} - (-1)^\ell \bar{\mathcal{R}\{h\}^{\ell,-m}}|^2}{4 \sum_{\ell,m} |h^{\ell,m}|^2}}. \quad (12b)$$

Because of this minimization, the result will be independent of the original attitude of the frame used to measure h by

⁸ We know of no way to eliminate the minimization process; as far as we know, some explicit numerical optimization is necessary. However, the problem is essentially two-dimensional, rather than the naive expectation of three-dimensional, because the result is insensitive to a final rotation about the z axis. This makes the procedure far more efficient. See the [ancillary materials](#) for more detail.

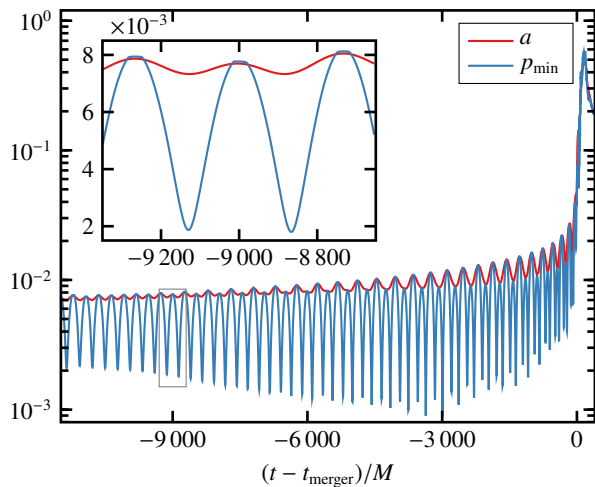


FIG. 2. **Rotationally invariant measures of asymmetry.** This plot shows the antisymmetry a defined in Eq. (9) and the minimal parity violation p_{\min} defined in Eq. (12), for the system described at the beginning of Sec. II. Because $p_{\min} \neq 0$, there is no frame in which the $h^{\ell,m}$ modes of this system satisfy Eq. (3).

construction. More specifically, when this value is nonzero—as in our chosen system—we know that there cannot be any frame in which Eq. (3) is satisfied.

Figure 2 shows the antisymmetry a and minimal parity violation p_{\min} for our chosen numerical system. Both curves are almost entirely determined by the $h^{2,\pm 2}$ and $h^{2,0}$ modes, as measured in the co-rotating frame. The antisymmetry starts out at roughly 0.7% at the beginning of the simulation, and increases very rapidly near merger, reaching 6% at the moment of merger, peaking near 60% shortly after merger. We note that the system shown here exhibits relatively modest precession; considerations from PN theory suggest that we may expect such antisymmetries to be roughly four times larger during the inspiral of strongly precessing systems.

Intriguingly, the axis which minimizes p_{\min} in Eq. (12) always lies extremely close to one of the basis axes of the co-rotating frame; during the inspiral, this optimal axis sometimes switches discontinuously to a direction close to a different basis axis of the co-rotating frame. We can see this in the inset of Fig. 2, which represents a little over one full orbit. There are brief periods, twice per orbit, during which p_{\min} and a nearly agree—in fact, p_{\min} is slightly larger, presumably due to the influence of modes with odd m . These correspond to times during which the $h^{2,\pm 2}$ modes are nearly equal and the minimal parity-violation axis is very nearly the \hat{Z} axis of the co-rotating frame. There is then a discontinuous change in the slope of the p_{\min} curve, as the parity violation along \hat{Z} remains large, but the violation along \hat{Y} drops, so the minimization of Eq. (12) switches to that axis. The parity projection along \hat{Y} is insensitive to the $h^{2,\pm 2}$ asymmetry.

While a and p_{\min} are *rotationally* invariant, they are not *translationally* invariant. In fact, the numerical data shown here come from a numerical simulation with a non-zero total

velocity in the initial data. We have removed this initial velocity for all data shown in this paper by transforming the asymptotic waveform data to counteract the velocity [38].⁹ The residual velocity of the initial data only has magnitude $\sim 6 \times 10^{-5} c$, and the boost transformation *per se* does not change the data appreciably. However, the resulting translation does have a significant effect on the waveform, reducing the asymmetry by an order of magnitude late in the inspiral despite the fact that the displacement is less than $\sim 1 M$ throughout the simulation. And although we set the initial velocity to be roughly zero, a recoil (hence also translation) develops in the data as the system approaches merger, which has noticeable effects. For example, in Fig. 2, successive peak values of p_{\min} are roughly equal near the beginning of the simulation; closer to merger, successive peaks are distinctly uneven. These are entirely consistent with the effects of translation.

The boost and spatial translation *cannot* be eliminated by extrapolation to infinite radius [13], Cauchy-characteristic evolution [14, 44–47], or any similar scheme. Rather, like time-translation and rotation, they are asymptotic symmetries of asymptotically flat spacetimes,¹⁰ and thus correspond to inherent gauge freedoms. We have simply chosen to impose a gauge condition on the NR data to coincide roughly with the PN gauge early in the simulation.

C. Waveform attitude

In addition to the rotationally invariant scalars introduced in the last section, we can also examine five quantities that transform as vectors under rotation. Three are defined with respect to the gravitational waves themselves. To define the first, we need the matrix [21]

$$\langle LL \rangle^{ab} := \sum_{\ell,m,m'} \bar{h}^{\ell,m'} \langle \ell, m' | L^a L^b | \ell, m \rangle h^{\ell,m}. \quad (13)$$

Here, the $|\ell, m\rangle$ represent the spin-weight $s = -2$ SWSH, on which the angular-momentum operator L^a acts just as in the non-spin-weighted case [18]. Our first vector is the dominant eigenvector of this matrix, labeled \hat{V}_h .¹¹ This can be thought of as the approximate symmetry axis of the waveform. We can also define another vector explicitly:

$$\langle L \partial_t \rangle^a := \sum_{\ell,m,m'} \Im \left[\bar{h}^{\ell,m'} \langle \ell, m' | L^a | \ell, m \rangle \partial_t h^{\ell,m} \right]. \quad (14)$$

⁹ That velocity is set to the ADM momentum divided by the ADM energy, where those quantities are measured in the initial data [39–43]. This is appropriate under the assumption that the initial-data slice contains no significant contribution to the ADM momentum and energy from anything other than the black holes themselves—for example junk radiation or gravitational waves intentionally included in the initial data.

¹⁰ In fact, the translations are part of a larger class of symmetries, deemed “supertranslations” [17, 48–51]. Combined with rotations and boosts, these comprise the general asymptotic symmetries of asymptotically flat spacetime—referred to as the Bondi–Metzner–Sachs (BMS) group [17, 48, 52].

¹¹ Because it is an eigenvector, the sign of \hat{V}_h is meaningless; we always choose it to lie more parallel than antiparallel to $\vec{\omega}$, defined in Eq. (15).

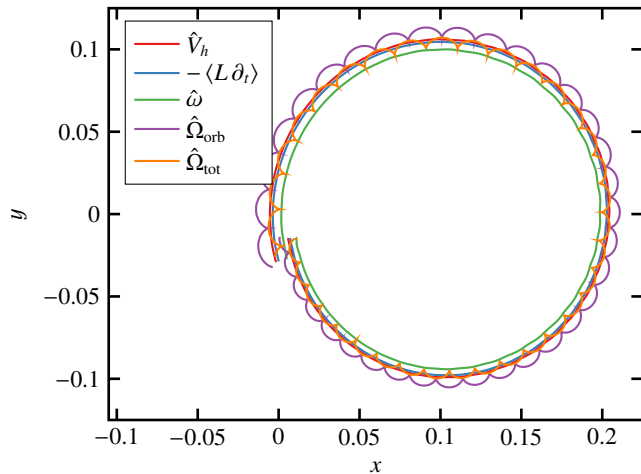


FIG. 3. **Vectors of a precessing system.** This plot shows the components of five important vectors for a precessing system. The curves evolve counterclockwise. The smooth curves are, from outer to inner, the waveform axis \hat{V}_h , the projection of waveform time dependence onto rotation $\langle L \partial_t \rangle$, and the waveform angular velocity $\hat{\omega}$. The scalloped curves are derived from the numerical coordinates and show the nutations of the precession. The outer curve is the *orbital* angular velocity of the binary $\hat{\ell}$; the inner one is the *total* angular velocity $\hat{\Omega}_{\text{tot}}$. The data shown are from the simulation described at the beginning of Sec. II, but only showing the first precession cycle (roughly the first 8000 M) for clarity. In a nonprecessing system, all five vectors coincide; here they are clearly distinct. We will see in Sec. III C that similar features are found in post-Newtonian results.

This quantity has the interpretation of the time derivative of the waveform projected into the “rotational” parts of the waveform [15], and is equal to the angular-momentum flux [53–57]. Finally, it is easy to derive the angular velocity of the waveform [15] using these expressions:¹²

$$\vec{\omega} = -\langle LL \rangle^{-1} \cdot \langle L \partial_t \rangle. \quad (15)$$

The directions of these three vectors are plotted in Fig. 3, appearing as the smooth curves. Intriguingly, none of the three vectors are aligned with any other at any time. Our usual notion of the waveform rotating about its alignment axis \hat{V}_h is incorrect. And the rotation axis of the waveform does not coincide with the axis of angular-momentum flux.

For comparison, we also plot the directions of two vectors relating to the dynamics of the binary, defined in terms of the coordinate positions of the black holes. Though these quantities are obviously gauge dependent, we will find it useful to make contact with PN theory using these vectors; the results from the numerical simulation are strikingly similar to the PN results. The orbital angular velocity $\vec{\Omega}_{\text{orb}}$ is given by the usual expression

$$\vec{\Omega}_{\text{orb}} = \hat{n} \times \dot{\hat{n}}, \quad (16)$$

¹² Incidentally, this is the angular velocity integrated to obtain the co-rotating frame used in plotting the modes in Fig. 1.

where \hat{n} is the separation vector between the two black holes. It is orthogonal to the orbital plane by definition, and describes the instantaneous velocity of the binary. We also need to distinguish the *total* angular velocity of the system $\vec{\Omega}_{\text{tot}}$. For precession to occur, $\vec{\Omega}_{\text{tot}}$ must also have a component $\vec{\Omega}_{\text{prec}}$ along \hat{n} ; essentially this additional component gives the angular velocity of the orbital angular velocity vector. We have

$$\vec{\Omega}_{\text{tot}} = \vec{\Omega}_{\text{orb}} + \vec{\Omega}_{\text{prec}}. \quad (17)$$

The directions of these two vectors are also plotted in Fig. 3, where they appear as the scalloped curves, as a result of the nutations of the system.

It is interesting to note that the dynamics of the system somehow conspire to eliminate the pronounced nutations of the orbital plane from the gravitational radiation, resulting in relatively smooth curves for all of the waveform vectors—though some oscillations are still visible on close inspection. This can be understood in terms of the analysis of Ref. [58], which used simple analogous systems to explain the nutations¹³ as occurring due to variations in the energy of different parts of a spinning object in motion transverse to the spin vector. The energy of the portion of the body in prograde motion increases, while the energy of the portion in retrograde motion decreases, so the center of mass-energy shifts depending on the direction of motion relative to the spin. But since the spin is roughly constant on an orbital timescale, this effect oscillates: the naive “coordinate” center of the black hole (as measured with reference to the horizon) moves relative to the center of mass-energy. Evidently, the centers of mass-energy are more relevant to the dynamics of the system, so we expect these to move on relatively smoother trajectories, while the coordinate centers nutate on the orbital timescale. Indeed, the black holes appear to nutate when considering only the coordinate positions of the horizons, as seen in the scalloped curves of Fig. 3. It is also evidently the non-nutating mass-energy that acts as the source of gravitational-wave emission, which is why the three curves in Fig. 3 measured from the waveforms are smooth.

The most basic point to take away from Fig. 3, though, is that there is no simple relationship between the directions of the orbital elements and various features in the waveforms. We will see in following sections that, to account for the non-alignment between the various curves in the figure, we must retain the asymmetric PN mode terms responsible for the effects shown above.

III. ASYMMETRIES IN PN THEORY

Each of the asymmetries demonstrated above can already be found in the PN literature, in some form, though they are often

¹³ The analysis of Ref. [58] suggests that systems whose spin components in the plane are aligned should exhibit nutations, in which the orbital plane tilts on a time scale much faster than precession; with spins anti-aligned, the effect would look more like “bobbing”, in which the orbital plane would move up and down.

obscure. To improve this situation, we first present a simplified framework for expressing the modes of the waveform, which allows for more tractable analytical expressions, as well as a robust, accurate and unified treatment of both precessing and nonprecessing systems. We then use this framework to describe the origins of the asymmetries in PN theory. Finally, we compare the results of PN calculations with the numerical results shown above.

A. Waveforms in the co-orbital frame

The standard framework for analyzing the radiation field of a black-hole binary uses symmetric trace-free (STF) tensors [59]. By taking various contractions between these tensors and vectors describing the position and attitude of an observer, we obtain the gravitational-wave field at the location of that observer. Alternatively, we can obtain the SWSH modes of the field by contracting with certain other STF spherical-harmonic tensors [59, 60]:

$$h^{\ell,m} \propto \left(U_L + i \frac{2\ell}{\ell+1} V_L \right) \mathcal{Y}_L^{\ell,-m}. \quad (18)$$

Here, U_L and V_L are referred to as radiative mass- and current-multipole tensors, the $\mathcal{Y}_L^{\ell,m}$ are spherical-harmonic tensors, and there is an implied summation over possible values of the multi-index L , which represents ℓ tensor components. U_L and V_L contain information about the physics of the system, whereas $\mathcal{Y}_L^{\ell,m}$ describes how a chosen coordinate system on the sphere relates to the modes. Therefore, choosing a coordinate system that relates directly to the physics can simplify the expressions for the modes; the modes can then be rotated to any other frame using Eq. (2).

The rank- ℓ tensors $\mathcal{Y}_L^{\ell,m}$ are given explicitly by Thorne [59]. Rather than reproducing the general expression here, we simply describe the most important features. Each such tensor contains m factors of $(\hat{x} - i\hat{y})$ [or $-m$ factors of $(\hat{x} + i\hat{y})$ for $m < 0$]. This factor is multiplied by a sum of terms involving n factors of the form δ_{jk} , for natural numbers $n \in \{0, \dots, \lfloor (\ell - m)/2 \rfloor\}$, with remaining factors given by \hat{z} as necessary for the tensor to have rank ℓ . There are two conclusions we need to draw from this. First is the obvious fact that these tensors are given in terms of the $(\hat{x}, \hat{y}, \hat{z})$ basis; contractions with arbitrary vectors could lead to very complicated expressions. Second, U_L or V_L can only contribute to a given $h^{\ell,m}$ mode if it has $|m| + 2n$ tensor components in the \hat{x} - \hat{y} plane for some natural number n .

The waveform multipole tensors U_L and V_L are generally given in terms of a vector basis $(\hat{n}, \hat{\lambda}, \hat{\ell})$ and the spin vectors of the black holes [23, 24, 28, 29, 59–63]. Here, \hat{n} is a vector pointing from one black hole to the other; $\hat{\lambda}$ is parallel to the time derivative $\dot{\hat{n}}$; and $\hat{\ell} = \hat{n} \times \hat{\lambda}$ is parallel to the orbital angular velocity $\vec{\Omega}_{\text{orb}}$. For example, we have the lowest-order

quadrupole contributions¹⁴

$$U_{jk} \propto \hat{n}_{\langle j} \hat{n}_{k\rangle} \quad (19a)$$

$$V_{jk} \propto \hat{\ell}_{\langle i} \hat{n}_{j\rangle}. \quad (19b)$$

They arise, respectively, from the familiar mass- and current-quadrupole source moments

$$I_{jk} \approx \int \rho x_{\langle j} x_{k\rangle} dV, \quad (20a)$$

$$J_{jk} \approx \int \rho x_a v_b \epsilon_{ab\langle j} x_{k\rangle} dV, \quad (20b)$$

where ρ is some effective density. At this level of approximation, and ignoring spin, we can think of ρ as just being the sum of a Dirac δ function for each of the two black holes—which is how the factors of x_j result in factors proportional to \hat{n}_j , and $x_a v_b \epsilon_{abj}$ results in a factor proportional to $\hat{\ell}_j$. These expressions, of course, only give a small flavor of the very complicated expressions necessary to calculate the waveform.

Multiplying the complexity of the waveform multipole tensors themselves, the general contractions of either expression in Eq. (19) with $\mathcal{Y}_{jk}^{2,m}$ will be quite complicated, involving numerous inner products like $\hat{n} \cdot \hat{z}$, and so on. For a precessing system measured in an inertial frame, this can quickly lead to enormously complicated expressions, even for fairly low-order harmonics [27]. The obvious solution, then, is to express the harmonics in a rotating frame $(\hat{X}, \hat{Y}, \hat{Z})$ that coincides with $(\hat{n}, \hat{\lambda}, \hat{\ell})$ at any instant. We refer to this as the “co-orbital” frame.

Using the co-orbital frame, we can return to the example of Eq. (19) and see the simplification at work. The two factors of U_{jk} now lie precisely in the \hat{X} - \hat{Y} plane, and so this term provides nonzero contributions to $h^{2,\pm 2}$ and $h^{2,0}$ only. Similarly, V_{jk} includes one factor in the \hat{X} - \hat{Y} plane and one along \hat{Z} , and so this term provides nonzero contributions to $h^{2,\pm 1}$ only. This separation of different components corresponding to different modes would not occur in a frame not aligned to the orbital elements; all modes would mix. Indeed, we will see in the following section that violations of exactly this separation of terms are the source of asymmetries, when factors of the spin vectors pointing in arbitrary directions replace the more orderly factors of \hat{n} , $\hat{\lambda}$, and $\hat{\ell}$.

Expressions for the spin terms in the gravitational-wave modes—which are the only terms containing asymmetries—are collected in Appendix A, including both symmetric and non-symmetric contributions. In Appendix B, we also exhibit formulas for efficiently evaluating the gravitational-wave polarizations measured by an inertial observer (such as a gravitational-wave detector), given the waveform in any rotating frame (such as the co-orbital frame). This allows us to skip the

¹⁴ Angle brackets indicate the symmetric trace-free (STF) part of the tensor, but that is unimportant to the argument; the tensors with which these are contracted are also STF and thus would give 0 on contraction with any non-STF part of the given quantities.

step of transforming the waveform into the inertial frame, which typically eliminates the need to calculate the many elements¹⁵ of the Wigner $\mathfrak{D}^{(\ell)}$ matrices.

B. Origin of asymmetry

We now have the tools necessary to understand exactly where the asymmetries come from. By taking the contractions between the tensors, Eq. (18) is also sometimes written [59, 60] as

$$h^{\ell,m} \propto (U^{\ell,m} - i V^{\ell,m}). \quad (21)$$

$U^{\ell,m}$ and $V^{\ell,m}$ are the radiative mass- and current-multipole modes. These modes individually have well defined parity behavior. Thorne [59] notes that the reality condition on h_+ and h_- implies the relations

$$U^{\ell,m} = (-1)^m \bar{U}^{\ell,-m}, \quad (22a)$$

$$V^{\ell,m} = (-1)^m \bar{V}^{\ell,-m}. \quad (22b)$$

This is an entirely immutable consequence of our choice of spin-weighted spherical harmonics and of the fact that distances are measured with real numbers. On the other hand, Blanchet *et al.* [64] report that

$$h^{\ell,m} = (-1)^\ell \bar{h}^{\ell,-m} \quad (23)$$

for the modes in the nonprecessing systems they treat. Note that the exponent here is ℓ , rather than m as in the preceding equations, and that the latter equation implies a conjugation of the factor of i that is explicitly present in Eq. (21). We saw in Sec. II B that this equation is equivalent to invariance of the system under reflection across the x - y plane. It must be emphasized that, unlike Eq. (22), this relation is not an essential truth, but merely a statement about modes in certain systems, assuming a certain attitude of the decomposition basis. It implies that the amplitudes of modes with equal ℓ and opposite m will necessarily be equal; the modes will be symmetric because $|h^{\ell,m}| = |(-1)^\ell \bar{h}^{\ell,-m}| = |h^{\ell,-m}|$. Thus, understanding mode asymmetry will require understanding why Eq. (23) is true for the modes of Ref. [64], and why it fails otherwise—or equivalently, finding terms that are not invariant under reflection across the x - y plane.

By simply inserting Eqs. (21) and (22) into Eq. (23), we can easily see that they are consistent if and only if the multipole modes satisfy

$$U^{\ell,m} = 0 \quad \text{for odd } \ell + m, \quad (24a)$$

$$V^{\ell,m} = 0 \quad \text{for even } \ell + m. \quad (24b)$$

And this is indeed the case for all such terms in nonprecessing systems [65]. Recall, as mentioned in Sec. III A, that $U^{\ell,m}$ and

$V^{\ell,m}$ can only be nonzero if the corresponding U_L or V_L has $|m| + 2n$ tensor components in the \hat{n} - $\hat{\lambda}$ plane, for some natural number n . This shows us how to find terms that cause mode asymmetry: for even ℓ , look for terms in U_L with an *odd* number of factors in the \hat{n} - $\hat{\lambda}$ plane, and terms in V_L with an *even* number of such factors—and contrariwise for odd ℓ .

The most important example comes from the lowest-order spin term, which appears in V_{jk} . As mentioned previously, this term arises from the current-quadrupole source moment given in Eq. (20b). This involves the integrand $\rho x_a v_b \epsilon_{abj}$, which just becomes the *orbital* angular momentum when spin is ignored. When spin is included, however, this factor gives rise to a term in the *spin* angular momentum. Incorporating this effect from both black holes, we can see that V_{jk} now includes a term proportional to $\Sigma_{(j} n_{k)}$, where the spin vector Σ_j was given below Eq. (5). When the spins are aligned with $\hat{\ell}$, this term is proportional to the basic V_{jk} expression in Eq. (19b), having just one factor in the \hat{n} - $\hat{\lambda}$ plane, and thus providing symmetric contributions to $h^{2,\pm 1}$ only. However, when $\vec{\Sigma}$ has any component in the \hat{n} - $\hat{\lambda}$ plane, it will behave more like U_{jk} as given in Eq. (19a). Thus, it will provide nonzero contributions to $h^{2,\pm 2}$ and $h^{2,0}$; because of the factor of i in Eq. (21), these contributions will necessarily be asymmetric.

We can also think of this in terms of the effect on Σ_j of the parity-conjugation operator P_Z , which reflects the system across the X - Y plane, and the more familiar parity-conjugation operator P_- , which reverses the signs of all (polar) vectors. Through unfortunate accidents of history and dimensionality [66], spin quantities like Σ_j are usually regarded as “axial” vectors, which do not change under P_- , as is well known. For spins aligned with \hat{Z} , this invariance extends to P_Z , which can also be regarded as P_- composed with a rotation through π about \hat{Z} . However, if the spin has any component orthogonal to \hat{Z} , the additional rotation imposed by P_Z will affect the direction of the spin. Thus, when Σ_j has a component in the X - Y plane, terms like $\Sigma_{(j} n_{k)}$ will not be invariant under P_Z , which means that Eq. (23) will not be true.

Interestingly, these terms also violate the standard result (valid for nonprecessing systems in an appropriate frame) that $h^{\ell,m} \propto \exp\{-i m \Phi\}$, where Φ is the orbital phase. Such phase factors usually come from contractions of the $\pm m$ factors of $(\hat{x} \mp i \hat{y})$ with the same number of factors of \hat{n} —which is considered in the standard analysis to be rotating in the \hat{x} - \hat{y} plane with phase Φ . However, for these spin terms, one factor of \hat{n} is replaced by $\vec{\Sigma}$, which is fairly constant on the orbital timescale, so its contraction with $(\hat{X} \mp i \hat{Y})$ will be roughly constant in the co-nutating frame. Thus, the complex phase of this spin contribution will vary with the orbital phase as $\exp\{-i(m \mp 1)\Phi\}$. Alternatively, in the co-orbital frame we have $\hat{n} = \hat{X}$, which leads to trivial contractions, but $\vec{\Sigma}$ rotates on an orbital timescale with phase $-\Phi$, leading to an overall phase of $\exp\{\mp i \Phi\}$. In either type of frame, the resulting phase factor is the source of the oscillations. And so, not only will asymmetries generally be present in waveforms from precessing systems, but they will oscillate on an orbital timescale, as seen in Sec. II. We will now show that the same features do indeed appear in PN data when

¹⁵ For example, there are 959 elements with $\ell \leq 8$, scaling roughly as ℓ^3 .

asymmetries are included.

C. Asymmetries in PN data

Using the asymmetric terms described above, we can construct a PN waveform corresponding to the numerical data discussed in Sec. II, and reproduce each of the plots given above to see if those features are also present in the PN waveform. A full comparison between NR and PN is beyond the scope of this paper; our purpose here is simply to show that the asymmetric PN terms are capable of reproducing the features seen in the numerical data.

The PN initial parameters are chosen naively, using the horizon quantities from the NR data measured roughly 800 M after the beginning of the simulation. This numerical data is taken with respect to the arbitrary coordinates in the strongly dynamical part of the spacetime. In particular, we do not expect the coordinates in the vicinities of the horizons to have any clear relation to coordinates at \mathcal{I}^+ —where the waveforms are ostensibly measured. Therefore, we align the PN waveform to the NR waveform by shifting in time and by rotating, to optimize the alignment between the waveform frames [15, 67].

In Fig. 4, we reproduce each of the plots from Sec. II, but use PN data. For comparison, the NR data are included as dotted curves of corresponding colors. Broadly speaking, the PN and NR results are qualitatively very similar. The antisymmetry and parity violation would be zero without the terms described above. By including them, we obtain features much like those seen in the numerical data. There are, of course, quantitative disagreements. For example, the overall PN amplitudes of the $h^{2,\pm 2}$ modes are larger than the NR amplitudes, while the size of the oscillations is very nearly correct (in both amplitude and phase). Similarly, while the vectors derived from the waveform precess far more smoothly than the nutating orbital vectors, there are larger oscillations present in the PN data than in the NR data. Of course, such disagreements are to be expected

from the approximate formulas of PN. The important point is that the agreement is drastically improved when antisymmetric terms are included in the PN formulas.

IV. ANTISYMMETRIES IN BINARY RECOIL

One of the most consequential discoveries of the era of numerical relativity was the discovery of “super-kicks” [68–73], in which the linear momentum carried off by gravitational waves from binaries with spins in the orbital plane can be so large that the merged system is left with a very large recoil velocity—possibly in excess of 5000 km s⁻¹ [73]. Linear momentum can only be carried off if the distribution of energy in the radiated waves is asymmetric. Our study of the asymmetry in gravitational radiation can therefore improve our understanding of the origin of the recoil.

Translating Thorne’s Eq. (4.18) [59] into our notation, we have the following expression for the linear-momentum flux in the form of gravitational waves:

$$\frac{d\vec{p}}{d\Omega dt} = \frac{R^2}{16\pi} \left| \frac{dh}{dt} \right|^2 \hat{r}, \quad (25)$$

where \hat{r} is the direction from the source to the point in question and R is the distance from the source to the observation sphere (so that Rh asymptotes to a nonzero constant). To find the total linear-momentum emission, we can integrate over all angles, expand the integrand in terms of the $h^{\ell,m}$ modes, and use the fact that each component of \hat{r} may be written as a sum of $\ell = 1$ spherical harmonics. Defining the modes $\hat{r}_j^{\ell,m}$ as implied by

$$\hat{r}_j = \sqrt{\frac{2\pi}{3}} \left(Y_{1,-1} - Y_{1,1}, iY_{1,-1} + iY_{1,1}, \sqrt{2}Y_{1,0} \right)_j, \quad (26)$$

we can do the integral explicitly, using a formula from Ref. [74], and find

$$\frac{dp_j}{dt} = \frac{R^2}{16\pi} \sum_{\ell,\ell',m,m'} \hat{r}_j^{1,m'-m} \dot{h}^{\ell,m} \bar{\dot{h}}^{\ell',m'} (-1)^{m'} \sqrt{\frac{3(2\ell+1)(2\ell'+1)}{4\pi}} \begin{pmatrix} \ell & \ell' & 1 \\ m & -m' & m' - m \end{pmatrix} \begin{pmatrix} \ell & \ell' & 1 \\ 2 & -2 & 0 \end{pmatrix}. \quad (27a)$$

We use $\dot{p}_j := dp_j/dt$ and $\dot{h} := dh/dt$ for brevity. For the particularly interesting case of the z component, this reduces to

$$\dot{p}_z = \frac{R^2}{16\pi} \sum_{\ell,\ell',m} \dot{h}^{\ell,m} \bar{\dot{h}}^{\ell',m} (-1)^m \sqrt{(2\ell+1)(2\ell'+1)} \begin{pmatrix} \ell & \ell' & 1 \\ m & -m & 0 \end{pmatrix} \begin{pmatrix} \ell & \ell' & 1 \\ 2 & -2 & 0 \end{pmatrix}. \quad (27b)$$

In each of these equations, the last two factors are Wigner’s 3 j symbols. Noting various properties of those symbols, we can see that the sums over ℓ' only run over $\{\ell - 1, \ell, \ell + 1\}$. We also know that the sum over m' in Eq. (27a) runs over $\{m - 1, m + 1\}$ for the x and y components, and reduces to $m' = 0$ for the z component. These facts limit mode mixing, and thus make the sum far more tractable. These expressions are independent

of any PN expansion, and are given directly in terms of the waveform modes, rather than the source multipoles.

For example, we can find all terms in Eq. (27b) to which the

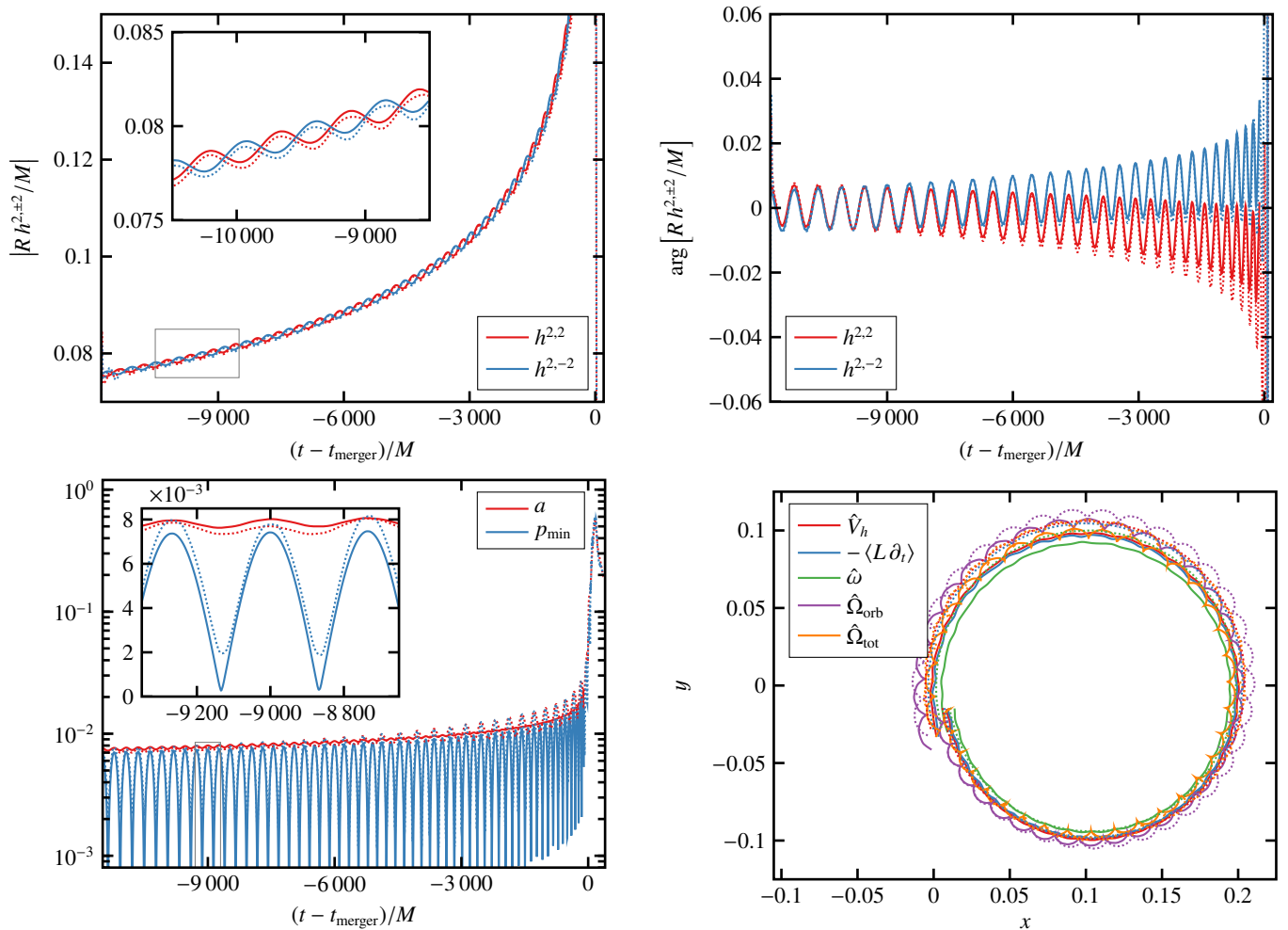


FIG. 4. **Comparing asymmetries in the NR and PN data.** These plots reproduce the preceding figures, but now show the PN data as solid curves, and the corresponding NR data as dotted curves. We see imperfect quantitative agreement, as must be expected of approximate analytical waveforms. For example, the overall PN amplitude is too large compared to NR (top left). Similarly, the PN p_{\min} is smaller than expected, while the a is larger than expected (bottom left). Nonetheless, the qualitative agreement is impressive, showing that each of the features described in the numerical data [Sec. III] is also present in the PN waveforms once the antisymmetric terms have been included.

$\dot{h}^{2,\pm 2}$ modes contribute:

$$\dot{p}_z = \frac{R^2}{12\pi} \left(|\dot{h}^{2,2}|^2 - |\dot{h}^{2,-2}|^2 \right) + \frac{R^2}{24\pi} \sqrt{\frac{5}{7}} \Re \left[\dot{h}^{2,2} \bar{\dot{h}}^{3,2} + \dot{h}^{2,-2} \bar{\dot{h}}^{3,-2} \right] + \dots, \quad (28)$$

where remaining terms do not involve $\dot{h}^{2,\pm 2}$. This equation is entirely general, independent of the frame used to decompose the waveform into modes and of any PN or other approximations. However, this result is particularly interesting in the co-orbital frame, because it expresses the linear momentum emitted by gravitational waves in a direction orthogonal to the orbital plane; this is the origin of “super-kicks”. The first term involves exactly the asymmetry visible in Figs. 1 and 2. Similarly, the second term would be zero if the $h^{2,\pm 2}$ and $h^{3,\pm 2}$

modes obeyed the parity-invariance equation, Eq. (3).¹⁶

The obvious parity violation evident in Eq. (27b) might tempt us to conjecture that only the antisymmetric portions of the waveform are involved in producing a recoil. In fact, we can show that this is not at all the case. To begin, we consider \dot{p}_j to be a functional operating on the waveform: $\dot{p}_j[h]$. We also define P_k to be any of the three involution operators (P_x, P_y, P_z). Using this notation, we expect on physical grounds to find

$$P_k \dot{p}_j[h] = \dot{p}_j[P_k h]. \quad (29)$$

That is, any parity inversion of the recoil produced by h is the same as the recoil produced by that parity inversion of h .

¹⁶ This is true for the z component of the momentum only. Similar terms appear in the expressions for the x and y components, and can be nonzero without violating Eq. (3). Those terms are the mechanism for emission of linear momentum from nonprecessing systems.

Though the physical interpretation is clear, it is not immediately obvious that our mathematical expressions for the recoil behave correctly under parity inversions. However, if we consider the integral of Eq. (25) needed to find $P_k \dot{p}_j[h]$, we can use $P_k \hat{r} = -\hat{r}$ and perform a change of variables, for which the Jacobian determinant is -1 , leaving us with an expression identical to that of $\dot{p}_j[P_k h]$ [75]. We can also verify this fact for the particular expressions in Eqs. (27) by inserting the various transformation formulas given in Eqs. (C10), relabeling the summation indices, and using properties of the Wigner $3j$ symbols.

As in Sec. II B, we define the projection operators $\Pi_k := \frac{1}{2}(1 - P_k)$, which retain only the portions of the waveform that reverse sign under P_k . We also introduce the complementary projection operators $\mathbb{I}_k := \frac{1}{2}(1 + P_k)$, which retain only the portions of the waveform that do not change under P_k . It is not hard to see that these projection operators result in eigenfunctions of the corresponding parity inversions:

$$P_k \Pi_k = -\Pi_k \quad \text{and} \quad P_k \mathbb{I}_k = \mathbb{I}_k. \quad (30)$$

Now, using Eq. (29), we have

$$P_k \dot{p}_j[\mathbb{I}_k h] = \dot{p}_j[P_k \mathbb{I}_k h] = \dot{p}_j[\mathbb{I}_k h]. \quad (31)$$

This says that the parity inverse of the recoil vector equals itself. When $j \neq k$, this doesn't tell us anything. However, when $j = k$, the sign of that component of the vector must reverse under parity inversion. Thus, we have

$$\dot{p}_j[\mathbb{I}_j h] = 0. \quad (32)$$

The same logic, using $\dot{p}_j[-h] = \dot{p}_j[h]$, shows that

$$\dot{p}_j[\Pi_j h] = 0. \quad (33)$$

Taken together, we can interpret these equations to say that recoil in a given direction requires parity-violating asymmetry in that direction, but recoil is not caused by the antisymmetric part alone; it is caused by the *interaction* of the parity-violating and parity-satisfying parts of the waveform. In fact, we can even rewrite Eq. (25) as

$$\frac{d\vec{p}}{dt} = \frac{R^2}{8\pi} \int \Re \left\{ \Pi_j h \overline{\Pi_j h} \right\} \hat{r} d\Omega, \quad (34)$$

which is valid for any choice of j , and shows explicitly that the net recoil is a product of the symmetric and antisymmetric parts of the waveform.

V. CONCLUSIONS

We have shown that gravitational waves from precessing black-hole binaries include features that are inherently asymmetric, in the sense that no rotation can eliminate them. The asymmetries are caused by the presence of spin components that are not aligned with the symmetry axis of the orbital motion. The effects on the waveforms can be very large, causing direction-dependent effects on the relative amplitude of greater

than 50% at merger. These asymmetries can already be found in some PN expressions for the metric perturbation—though, in the literature, the expressions are generally simplified to eliminate asymmetries before being translated into modes. We separated the symmetric and anti-symmetric components of the waveform, and showed that neither component alone is responsible for binary recoil. Rather, binary recoil is a result of the interaction between the completely symmetric and the completely anti-symmetric components of the gravitational radiation.

We showed that the co-orbital frame significantly simplifies expressions for the PN waveform modes, without any approximations of small precession angles, *etc.* Because the attitude of the co-orbital frame must be calculated for any precessing system, there is no computational overhead in this approach—only savings from the simplified expressions. By computing the symmetric and anti-symmetric components of the waveforms separately, we can regain the efficiency of simultaneously calculating the $h^{\ell,m}$ and $h^{\ell,-m}$ mode pairs, which is used for nonprecessing systems [see Appendix A]. Finally, as demonstrated in Appendix B, it is possible to use modes expressed in the co-orbital frame (or any rotating frame) *directly* in calculation of the waveform observed by an inertial detector, rather than going through the computationally burdensome step of rotating the modes.

We suggest, therefore, that analyzing analytical mode expressions in the co-orbital frame and separating the symmetric from the anti-symmetric components lead to improvements in both the analytical treatment of waveforms and the numerical performance of related calculations. This will be important for gravitational-wave astronomy, so that these fascinating sources may be studied in greater detail and with higher accuracy. Precession imprints information on the gravitational-wave signal, which can potentially allow measurement of otherwise ambiguous features of astrophysical sources, and thus improve the scientific output of gravitational-wave astronomy [5].

Future work will be needed to improve the coverage of PN terms for precessing waveforms, and to draw numerical and analytical work closer. In particular, more extensive comparisons of PN and NR predictions are needed. The rough results shown in Sec. III C are only meant to be qualitative; they are tainted most prominently by the naive method used to determine the parameters of the PN system from coordinate-dependent quantities in the numerical data.

All of the methods and results of this paper are included as computer code in the [ancillary files](#) on this paper's arXiv page. These include the expressions for the waveform modes, code to evolve precessing binaries and compute the modes in the co-orbital frame, and code to transform and evaluate those modes. We hope that this may form a basis for future work.

ACKNOWLEDGMENTS

It is our pleasure to thank Jeandrew Brink, Geoffrey Lovelace, and Saul Teukolsky for useful conversations. This project was supported in part by the Sherman Fairchild Foundation; by NSF

Grants No. PHY-1306125 and AST-1333129; and by NSERC of Canada and the Canada Research Chairs Program.

The computations presented in this paper were performed on the Zwicky cluster hosted at Caltech by the Center for Advanced Computing Research, which was funded by the Sherman Fairchild Foundation and the NSF MRI-R² program; and on the GPC and Gravity clusters at the SciNet HPC Consortium [76], funded by: the Canada Foundation for Innovation under the auspices of Compute Canada; the Government of Ontario; Ontario Research Fund—Research Excellence; and the University of Toronto.

Appendix A: Waveform modes with asymmetric contributions

We now give the formulas for the contributions to the waveform modes from spins in the co-orbital frame. This form of the modes is useful as it is particularly simple; it factors out the dependence on attitude of the precessing binary including all orbital motion. Also, we can simply add these expressions directly to the equivalent non-spin mode contributions, to achieve more complete and accurate results. The combination may not be at a consistent PN order—since terms with spin will only be kept up to 2PN, while terms without may be kept up to 3.5PN—but the results will be numerically accurate, and will smoothly transition from nonprecessing to strongly precessing. Finally, calculating these modes numerically is efficient, as the symmetric and antisymmetric parts may be calculated separately, and then added with appropriate signs and conjugations to give both $h^{\ell,m}$ and $h^{\ell,-m}$, rather than calculating each individually.

We begin by defining the various elements. The black holes have masses M_1 and M_2 , and spins \vec{S}_1 and \vec{S}_2 , respectively. The additional symbols we will use in writing the modes are

$$M := M_1 + M_2, \quad (\text{A1a})$$

$$\nu := \frac{M_1 M_2}{M^2}, \quad (\text{A1b})$$

$$\delta := \frac{M_1 - M_2}{M}, \quad (\text{A1c})$$

$$\vec{S} := \vec{S}_1 + \vec{S}_2, \quad (\text{A1d})$$

$$\vec{\Sigma} := M \left(\frac{\vec{S}_2}{M_2} - \frac{\vec{S}_1}{M_1} \right), \quad (\text{A1e})$$

$$v := \left(M \left| \vec{\Omega}_{\text{orb}} \right| \right)^{1/3} = \sqrt{x}. \quad (\text{A1f})$$

The last symbol is the usual PN-expansion parameter, and we have set $G = c = 1$. Again, we note that \hat{n} is a unit vector pointing from black hole 2 to black hole 1; $\hat{\lambda}$ is a unit vector in the direction of $\frac{d}{dt}\hat{n}$; and $\hat{\ell} = \hat{n} \times \hat{\lambda}$.

The modes are derived from expressions for the metric perturbation h_{jk} , as given by Eqs. (4.9) of Ref. [24] and Eqs. (4.13) and (4.15) of Ref. [28]. These include the spin-orbit, $\text{spin}_1\text{-spin}_2$, spin_1^2 , and spin_2^2 terms through 2PN order, relative to the leading-order (non-spin) term in the metric perturbation. Using the substitutions $(\hat{n}, \hat{\lambda}, \hat{\ell}) \mapsto (\hat{x}, \hat{y}, \hat{z})$, the complex h field is derived from h_{jk} as

$$h := \frac{1}{2} \left[(\varphi^j \varphi^k - \vartheta^j \vartheta^k) + i (\vartheta^j \varphi^k + \varphi^j \vartheta^k) \right] h_{jk}, \quad (\text{A2})$$

where ϑ and φ are the usual spherical coordinates of the $(\hat{n}, \hat{\lambda}, \hat{\ell}) = (\hat{x}, \hat{y}, \hat{z})$ system. Equation (A2) expresses $h = h_+ - ih_\times$, so h is a field of spin weight $s = -2$. Note that there are many subtly different conventions throughout the literature for the various quantities we treat here. Our choices are internally consistent, and made so that the results for the modes given in Eq. (A5) are consistent with other results for *gravitational-wave modes* in the literature—specifically the review in Ref. [60]. Note in particular the relation between the field point φ in our co-orbital frame and the orbital phase Φ in the more common frame for which the system orbits in the x - y plane while the field point is in the y - z plane: formulas given in the two frames can be equated when we define $\varphi = \pi/2 - \Phi$.

We then find the SWSH mode decomposition according to

$$h^{\ell,m} := \int_0^\pi \int_0^{2\pi} h(\vartheta, \varphi) {}_{-2}\bar{Y}_{\ell,m}(\vartheta, \varphi) d\varphi \sin \vartheta d\vartheta. \quad (\text{A3})$$

As is standard, we rescale all modes by the leading-order (non-spin) term in $h^{2,2}$; that is, we present modes of the rescaled field

$$\hat{h} := \frac{1}{8\nu v^2} \sqrt{\frac{5}{\pi}} \frac{R}{M} h. \quad (\text{A4})$$

The results are the modes in the co-orbital frame [see Sec. III A]. These modes can, of course, be rotated into any other frame (including inertial and co-rotating frames) using Eq. (2).

For presentation purposes, we display each term in the form $\{\Pi_z h\} + \{\Pi_\times h\}$; the first brace group is symmetric (does not change sign) under reflection across the orbital plane, while the second is antisymmetric. Of course, these parts need not be recalculated for each mode. The terms may be calculated separately for modes with positive m , and the modes with corresponding $-m$ value constructed simply by combining the two types of terms after the appropriate conjugations and sign changes. We include the symmetric contributions to the modes coming from spin for completeness, even though they are essentially available from other sources [77]. The full expressions, including contributions from non-spin parts, are given in Mathematica and IPython notebooks available in the [ancillary materials](#) on this paper's arXiv page, along with code that computes the PN trajectories and produces the full PN waveform.

$$\hat{h}_{\text{spin}}^{2,-2} = \left\{ -\frac{2v^3(3S_\ell + \delta\Sigma_\ell)}{3M^2} + \frac{v^4(-22S_{1n}S_{2n} + 15iS_{1\lambda}S_{2n} + 12S_{1\ell}S_{2\ell} + 15iS_{1n}S_{2\lambda} + 10S_{1\lambda}S_{2\lambda})}{6M^4v} \right\} + \left\{ \frac{v^2(\Sigma_\lambda - i\Sigma_n)}{2M^2} + \frac{v^4[182i\delta S_n - 19\delta S_\lambda + 14i(7 - 20v)\Sigma_n - (5 - 43v)\Sigma_\lambda]}{84M^2} \right\} \quad (\text{A5a})$$

$$\hat{h}_{\text{spin}}^{2,-1} = \left\{ -\frac{iv^2\Sigma_\ell}{2M^2} + \frac{iv^4[86\delta S_\ell + (79 - 139v)\Sigma_\ell]}{42M^2} \right\} + \left\{ \frac{v^3(-25S_n + 4iS_\lambda - 13\delta\Sigma_n + 4i\delta\Sigma_\lambda)}{6M^2} + \frac{3v^4(S_{1\ell}S_{2n} + S_{1n}S_{2\ell})}{2M^4v} \right\} \quad (\text{A5b})$$

$$\hat{h}_{\text{spin}}^{2,0} = \left\{ \frac{\sqrt{\frac{2}{3}}v^4(S_{1n}S_{2n} - S_{1\lambda}S_{2\lambda})}{M^4v} \right\} + \left\{ \frac{iv^2\Sigma_n}{\sqrt{6}M^2} + \frac{iv^4[255\delta S_n + (45 - 506v)\Sigma_n]}{21\sqrt{6}M^2} \right\} \quad (\text{A5c})$$

$$\hat{h}_{\text{spin}}^{2,1} = \left\{ \frac{iv^2\Sigma_\ell}{2M^2} - \frac{iv^4[86\delta S_\ell + (79 - 139v)\Sigma_\ell]}{42M^2} \right\} + \left\{ \frac{v^3(25S_n + 4iS_\lambda + 13\delta\Sigma_n + 4i\delta\Sigma_\lambda)}{6M^2} - \frac{3v^4(S_{1\ell}S_{2n} + S_{1n}S_{2\ell})}{2M^4v} \right\} \quad (\text{A5d})$$

$$\hat{h}_{\text{spin}}^{2,2} = \left\{ -\frac{2v^3(3S_\ell + \delta\Sigma_\ell)}{3M^2} + \frac{v^4(-22S_{1n}S_{2n} - 15iS_{1\lambda}S_{2n} + 12S_{1\ell}S_{2\ell} - 15iS_{1n}S_{2\lambda} + 10S_{1\lambda}S_{2\lambda})}{6M^4v} \right\} + \left\{ -\frac{v^2(\Sigma_\lambda + i\Sigma_n)}{2M^2} + \frac{v^4[182i\delta S_n + 19\delta S_\lambda + 14i(7 - 20v)\Sigma_n + (5 - 43v)\Sigma_\lambda]}{84M^2} \right\} \quad (\text{A5e})$$

$$\hat{h}_{\text{spin}}^{3,-3} = \left\{ \frac{3i\sqrt{\frac{15}{14}}v^4[7\delta S_\ell + (3 - 9v)\Sigma_\ell]}{8M^2} \right\} + \left\{ -\frac{\sqrt{\frac{10}{21}}v^3[S_n + iS_\lambda + \delta(\Sigma_n + i\Sigma_\lambda)]}{M^2} \right\} \quad (\text{A5f})$$

$$\hat{h}_{\text{spin}}^{3,-2} = \left\{ -\frac{2\sqrt{\frac{5}{7}}v^3(S_\ell + \delta\Sigma_\ell)}{3M^2} \right\} + \left\{ \frac{\sqrt{\frac{5}{7}}v^4[25\delta(4iS_n + S_\lambda) + 4i(13 - 55v)\Sigma_n + (17 - 83v)\Sigma_\lambda]}{24M^2} \right\} \quad (\text{A5g})$$

$$\hat{h}_{\text{spin}}^{3,-1} = \left\{ \frac{iv^4[\delta S_\ell + (5 - 15v)\Sigma_\ell]}{24\sqrt{14}M^2} \right\} + \left\{ \frac{\sqrt{\frac{2}{7}}v^3[S_n - iS_\lambda + \delta(\Sigma_n - i\Sigma_\lambda)]}{3M^2} \right\} \quad (\text{A5h})$$

$$\hat{h}_{\text{spin}}^{3,0} = \{0\} + \left\{ -\frac{v^4[17\delta S_\lambda + (9 - 35v)\Sigma_\lambda]}{4\sqrt{42}M^2} \right\} \quad (\text{A5i})$$

$$\hat{h}_{\text{spin}}^{3,1} = \left\{ \frac{iv^4[\delta S_\ell + (5 - 15v)\Sigma_\ell]}{24\sqrt{14}M^2} \right\} + \left\{ \frac{\sqrt{\frac{2}{7}}v^3[S_n + iS_\lambda + \delta(\Sigma_n + i\Sigma_\lambda)]}{3M^2} \right\} \quad (\text{A5j})$$

$$\hat{h}_{\text{spin}}^{3,2} = \left\{ \frac{2\sqrt{\frac{5}{7}}v^3(S_\ell + \delta\Sigma_\ell)}{3M^2} \right\} + \left\{ \frac{\sqrt{\frac{5}{7}}v^4[25\delta(-4iS_n + S_\lambda) - 4i(13 - 55v)\Sigma_n + (17 - 83v)\Sigma_\lambda]}{24M^2} \right\} \quad (\text{A5k})$$

$$\hat{h}_{\text{spin}}^{3,3} = \left\{ \frac{3i\sqrt{\frac{15}{14}}v^4[7\delta S_\ell + (3 - 9v)\Sigma_\ell]}{8M^2} \right\} + \left\{ -\frac{\sqrt{\frac{10}{21}}v^3[S_n - iS_\lambda + \delta(\Sigma_n - i\Sigma_\lambda)]}{M^2} \right\} \quad (\text{A5l})$$

$$\hat{h}_{\text{spin}}^{4,-4} = \{0\} + \left\{ -\frac{9\sqrt{\frac{5}{7}}v^4[\delta(S_\lambda - iS_n) + (1 - 3v)(\Sigma_\lambda - i\Sigma_n)]}{8M^2} \right\} \quad (\text{A5m})$$

$$\hat{h}_{\text{spin}}^{4,-3} = \left\{ \frac{9i\sqrt{\frac{5}{14}}v^4[\delta S_\ell + (1 - 3v)\Sigma_\ell]}{8M^2} \right\} + \{0\} \quad (\text{A5n})$$

$$\hat{h}_{\text{spin}}^{4,-2} = \{0\} + \left\{ -\frac{\sqrt{5}v^4 [\delta(13S_\lambda + 14iS_n) + (1-3\nu)(13\Sigma_\lambda + 14i\Sigma_n)]}{168M^2} \right\} \quad (\text{A5o})$$

$$\hat{h}_{\text{spin}}^{4,-1} = \left\{ -\frac{i\sqrt{\frac{5}{2}}v^4 [\delta S_\ell + (1-3\nu)\Sigma_\ell]}{168M^2} \right\} + \{0\} \quad (\text{A5p})$$

$$\hat{h}_{\text{spin}}^{4,0} = \{0\} + \left\{ \frac{iv^4 [\delta S_n + (1-3\nu)\Sigma_n]}{84\sqrt{2}M^2} \right\} \quad (\text{A5q})$$

$$\hat{h}_{\text{spin}}^{4,1} = \left\{ \frac{i\sqrt{\frac{5}{2}}v^4 [\delta S_\ell + (1-3\nu)\Sigma_\ell]}{168M^2} \right\} + \{0\} \quad (\text{A5r})$$

$$\hat{h}_{\text{spin}}^{4,2} = \{0\} + \left\{ \frac{\sqrt{5}v^4 [\delta(13S_\lambda - 14iS_n) + (1-3\nu)(13\Sigma_\lambda - 14i\Sigma_n)]}{168M^2} \right\} \quad (\text{A5s})$$

$$\hat{h}_{\text{spin}}^{4,3} = \left\{ -\frac{9i\sqrt{\frac{5}{14}}v^4 [\delta S_\ell + (1-3\nu)\Sigma_\ell]}{8M^2} \right\} + \{0\} \quad (\text{A5t})$$

$$\hat{h}_{\text{spin}}^{4,4} = \{0\} + \left\{ \frac{9\sqrt{\frac{5}{7}}v^4 [\delta(S_\lambda + iS_n) + (1-3\nu)(\Sigma_\lambda + i\Sigma_n)]}{8M^2} \right\} \quad (\text{A5u})$$

Some of these terms were present in the mode decompositions given in Ref. [27]. By taking $\iota = 0$, $\Psi = 0$, and $\alpha = -\pi/2$ in that reference, and noting that their conventions for the polarization tensor give rise to relative factors of $(-i)^m$, we find agreement with all of the corresponding terms given here.

Appendix B: Efficient calculation of waveforms from rotating frames for data analysis

As mentioned previously, it is a simple matter to transform the waveform between frames using Eq. (2). For example, we might transform the waveform \hat{h} from the co-orbital frame back into h as seen in the inertial frame, and then evaluate the waveform at a point, to give us the data that would be measured by a gravitational-wave detector. But this is very computationally expensive if the end goal is simply to obtain the waveform along a single world line. Even if we only include the $\ell = 2$ component, rotation of the waveform requires calculating all 25 elements of the $\mathfrak{D}^{(2)}$ matrix; including through $\ell = 8$ would require calculating 959 elements of the various $\mathfrak{D}^{(\ell)}$ matrices. And because the rotation R changes from instant to instant, these calculations would all need to be redone at each time step. The waveform h in the inertial frame would then be evaluated as

$$h(\vartheta, \varphi) = \sum_{\ell, m} h^{\ell, m} {}_{-2}Y_{\ell, m}(\vartheta, \varphi). \quad (\text{B1})$$

The SWSH components in this expression would only need to be calculated once per waveform, and there are only 5 to evaluate for the $\ell = 2$ component, or 77 when including through

$\ell = 8$, so this would be a very small portion of the computation.

Fortunately, there is a far better alternative. We can evaluate the waveform as given in the co-orbital (or any other) frame, but change the point at which the evaluation takes place, to cancel out the rotation. This would require no evaluations of $\mathfrak{D}^{(\ell)}$ matrices, but 5 (77) evaluations of the SWSH components at each time step when including all modes through $\ell = 2$ ($\ell = 8$). This is a substantial savings, and could easily be implemented using existing software packages—for example, the SPINFAST package [78] developed for the cosmic-microwave-background community, or the SPHERICALFUNCTIONS module included in the **ancillary files** on this paper’s arXiv page.

One subtlety must be handled carefully. We would write the waveform in the inertial frame as

$$h(\vartheta, \varphi) = \sum_{\ell, m} \hat{h}^{\ell, m} {}_{-2}Y_{\ell, m}(\hat{\vartheta}, \hat{\varphi}) e^{2i\hat{\gamma}}, \quad (\text{B2})$$

where not only $(\hat{\vartheta}, \hat{\varphi})$ must be computed, but also the angle $\hat{\gamma}$. The latter is necessary because we must evaluate the spin-weighted field with respect to the tangent basis that would be used at the inertial point (ϑ, φ) . But the tangent basis of the ${}_{-2}Y_{\ell, m}$ function is defined naively, with respect to the input arguments $(\hat{\vartheta}, \hat{\varphi})$, and would therefore change from moment to moment in ways completely unrelated to the inertial tangent basis.¹⁷ Unless we account for $\hat{\gamma}$, our predicted waveform would

¹⁷ Another way of saying this is to note that, unlike the SWSH modes $h^{\ell, m}$, the SWSHs functions ${}_{-2}Y_{\ell, m}$ do not transform among themselves under rotations [15]; only the full $\mathfrak{D}_{m' m}^{(\ell)}$ functions do that, which is why we must use them in what follows.

be different from the physical waveform by an arbitrary and erratically time-dependent phase [22]—equivalent to a wildly rotating detector.

We can evaluate the right-hand side above, using the expression for SWSHs in terms of the Wigner \mathfrak{D} matrices:

$${}_s Y_{\ell,m}(\vartheta, \varphi) = (-1)^s \sqrt{\frac{2\ell+1}{4\pi}} \mathfrak{D}_{m,-s}^{(\ell)}(R_{\vartheta,\varphi}), \quad (\text{B3})$$

where $R_{\vartheta,\varphi}$ rotates \hat{z} onto the point with coordinates (ϑ, φ) . Now, combining this with Eqs. (2) and (B1), we can calculate

$$h(\vartheta, \varphi) = \sum_{\ell,m} h^{\ell,m} {}_{-2}Y_{\ell,m}(\vartheta, \varphi) \quad (\text{B4a})$$

$$= \sum_{\ell,m} \sum_{m'} \hat{h}^{\ell,m'} \mathfrak{D}_{m',m}^{(\ell)}(R_f^{-1}) \sqrt{\frac{2\ell+1}{4\pi}} \mathfrak{D}_{m,2}^{(\ell)}(R_{\vartheta,\varphi}) \quad (\text{B4b})$$

$$= \sum_{\ell,m} \hat{h}^{\ell,m} \sqrt{\frac{2\ell+1}{4\pi}} \mathfrak{D}_{m,2}^{(\ell)}(R_f^{-1} R_{\vartheta,\varphi}). \quad (\text{B4c})$$

Here, R_f is the rotation that takes the inertial frame onto the rotating frame, and we have used the composition property of the $\mathfrak{D}^{(\ell)}$ matrices to combine two into one.

We emphasize that Eq. (B4c) is the preferred way to evaluate $h(\vartheta, \varphi)$, since evaluation of the general SWSH is essentially the same as evaluating elements of the Wigner $\mathfrak{D}^{(\ell)}$ matrix, in terms of computational cost. Moreover, the `SPHERICALFUNCTIONS` module implements efficient and stable evaluation of the $\mathfrak{D}^{(\ell)}$ matrices directly in terms of quaternions, meaning that the product $R_f^{-1} R_{\vartheta,\varphi}$ can be evaluated by simple quaternion multiplication. The accompanying `GWFRAMES` module uses this technique for evaluating rotating-frame waveforms at a point.

Although Eq. (B4c) is a far superior formula for calculating $h(\vartheta, \varphi)$, it may also be useful for testing purposes or for working with older software libraries to rewrite the result in precisely the terms of Eq. (B2). We caution, however, that this is tantamount to using Euler angles. To be precise, $(\hat{\varphi}, \hat{\vartheta}, \hat{\gamma})$ [note the ordering] is the Euler-angle form of the rotation $R_f^{-1} R_{\vartheta,\varphi}$ under the z - y - z convention [15]. Of course, the Euler-angle representation of rotations is dramatically inferior to quaternions in almost every way—in this case, because composing rotations given in terms of Euler angles is computationally expensive and inaccurate (essentially requiring conversion to another form and back), and because the $\mathfrak{D}^{(\ell)}$ matrices can be calculated more accurately and efficiently using quaternions directly. Nonetheless, we can at least reduce one obstacle on this path by showing how to derive the angles after composing the rotations by quaternion multiplication.

We need to calculate $\hat{\vartheta}$, $\hat{\varphi}$, and $\hat{\gamma}$ such that

$$R_f^{-1} R_{\vartheta,\varphi} = R_{\hat{\vartheta},\hat{\varphi}} e^{\hat{\gamma}\hat{z}/2}. \quad (\text{B5})$$

In the last term on the right-hand side of this equation, we have used quaternion notation to express a rotation through $\hat{\gamma}$ about

the z axis.¹⁸ Now, we know both quantities on the left-hand side of the equation, so we can simply evaluate their product, and define the quaternion components of the result as (r_0, r_1, r_2, r_3) . Straightforward calculation shows that our angles are given by the following simple formulas:

$$\hat{\vartheta} = 2 \arccos \sqrt{r_0^2 + r_3^2}, \quad (\text{B6a})$$

$$\hat{\varphi} = \arctan \frac{r_3}{r_0} + \arctan \frac{-r_1}{r_2}, \quad (\text{B6b})$$

$$\hat{\gamma} = \arctan \frac{r_3}{r_0} - \arctan \frac{-r_1}{r_2}. \quad (\text{B6c})$$

Using these results, Eq. (B4) becomes

$$h(\vartheta, \varphi) = \sum_{\ell,m} \hat{h}^{\ell,m} \sqrt{\frac{2\ell+1}{4\pi}} \mathfrak{D}_{m,2}^{(\ell)}(R_{\hat{\vartheta},\hat{\varphi}} e^{\hat{\gamma}\hat{z}/2}) \quad (\text{B7a})$$

$$= \sum_{\ell,m} \hat{h}^{\ell,m} \sqrt{\frac{2\ell+1}{4\pi}} \mathfrak{D}_{m,2}^{(\ell)}(R_{\hat{\vartheta},\hat{\varphi}}) e^{2i\hat{\gamma}} \quad (\text{B7b})$$

$$= e^{2i\hat{\gamma}} \sum_{\ell,m} \hat{h}^{\ell,m} {}_{-2}Y_{\ell,m}(\hat{\vartheta}, \hat{\varphi}). \quad (\text{B7c})$$

In going from the first to the second line, we have used the composition property of the $\mathfrak{D}^{(\ell)}$ matrices, and the simple expression $\mathfrak{D}_{m',2}^{(\ell)}(e^{\hat{\gamma}\hat{z}/2}) = e^{2i\hat{\gamma}} \delta_{m',2}$. The sum in Eq. (B7c) is precisely the naive evaluation of the waveform in the rotating frame, which may be readily available from certain software packages.

Again, we discourage the use of Eq. (B7c), as it requires the additional intermediate calculations of Eqs. (B6), along with the usual numerical inaccuracies and edge cases to deal with; we advise using Eq. (B4c) instead, with direct evaluation of the $\mathfrak{D}^{(\ell)}$ matrices in terms of quaternions. However, either expression eliminates the need to rotate the waveform modes themselves, which reduces the number of $\mathfrak{D}^{(\ell)}$ elements needed by an order of magnitude at each time step. Because the complete expressions for the PN waveform are nearly as simple as the expressions for nonprecessing systems, and because the system's orbital trajectories (R_f , here) needed to be calculated in any case, this gives us an efficient method for producing an accurate waveform for use in data analysis. While this will presumably still be computationally expensive compared to using simple quadrupolar waveforms, whenever higher modes or generally greater accuracy are needed, this approach can be faster and more accurate than using expressions for waveforms in which the rotation is explicitly included.

Appendix C: Parity and antipodes

It is vital to understand in detail the behavior of waveforms and—in particular—the SWSH modes of waveforms under

¹⁸ Essentially, \hat{z} is the generator of rotations about the z axis, and a unit quaternion is equivalent to the square-root of the usual rotation matrix—hence the factor of $1/2$. For a more complete explanation of quaternions as applied to rotations, see Sec. I C or Appendix A of Ref. [15].

parity conjugation and evaluation at antipodes. Here, we describe these details in greater generality than is necessary for our purposes in the main body of this paper, in the hope that this more complete view will clarify the issues involved.

We begin by defining the three parity operators P_x , P_y , and P_z , which represent reflections along the given axes. So, for example, P_z represents reflection across the x - y plane; vectors under this operation just get a sign flip in the z component. We denote by P_- the more standard parity operation in three-dimensional physics, which is reversal of all components of a vector. Equivalently, P_- is the composition of the previous three operations, or any one of them followed by rotation through π about that same axis. For simplicity, we denote any one of these four operators as P_i .

For a spin-zero field f , its parity-conjugate field is found by simply evaluating the original field at the parity-conjugate location. Thus, for any direction \hat{r} , we can relate the values of the field f and its parity-conjugate field $P_i\{f\}$ as

$$P_i\{f\}(\hat{r}) = f(P_i\{\hat{r}\}). \quad (\text{C1})$$

In this sense, spin-zero fields transform as ‘‘true scalars’’.

Spin-weighted fields, on the other hand, do not transform so simply, because they are defined with respect to a coordinate basis for the tangent space of the sphere, and that basis is also affected by the parity operation. In terms of the standard $(\hat{\theta}, \hat{\phi})$ basis, we have the following transformations:

$$P_x : \hat{\theta}(\hat{r}) \mapsto \hat{\theta}(P_x\hat{r}) \quad P_x : \hat{\phi}(\hat{r}) \mapsto -\hat{\phi}(P_x\hat{r}), \quad (\text{C2a})$$

$$P_y : \hat{\theta}(\hat{r}) \mapsto \hat{\theta}(P_y\hat{r}) \quad P_y : \hat{\phi}(\hat{r}) \mapsto -\hat{\phi}(P_y\hat{r}), \quad (\text{C2b})$$

$$P_z : \hat{\theta}(\hat{r}) \mapsto -\hat{\theta}(P_z\hat{r}) \quad P_z : \hat{\phi}(\hat{r}) \mapsto \hat{\phi}(P_z\hat{r}), \quad (\text{C2c})$$

$$P_- : \hat{\theta}(\hat{r}) \mapsto -\hat{\theta}(P_-\hat{r}) \quad P_- : \hat{\phi}(\hat{r}) \mapsto \hat{\phi}(P_-\hat{r}). \quad (\text{C2d})$$

Thus, the usual complex basis representation $m_j := \vartheta_j + i\varphi_j$ transforms under these parity operations as

$$P_x, P_y : m_j \mapsto \bar{m}_j, \quad (\text{C3a})$$

$$P_z, P_- : m_j \mapsto -\bar{m}_j. \quad (\text{C3b})$$

Since h has spin weight $s = -2$, it is defined by contraction of a tensor field with two copies of \bar{m} , parity conjugation simply induces complex conjugation of the field:

$$P_i\{h\}(\hat{r}) = \bar{h}(P_i\{\hat{r}\}). \quad (\text{C4})$$

This is distinct from the transformation of spin-zero fields (C1) only by virtue of the complex conjugation on the right-hand side. It is worth noting that similar expressions for spin weight $s = -1$ fields, for example, would also involve factors of -1 for P_z and P_- .

We can also distinguish the parity operations from a similar operation: evaluation at the antipode, which we denote by A . The distinction is important because the tangent basis used for evaluation at the antipode is just the standard basis at that point; the vectors are not affected by the operation A , as they are for the P_i operations. Thus,

$$A\{f\}(\hat{r}) = f(A\{\hat{r}\}) = f(-\hat{r}), \quad (\text{C5})$$

for a field of *any* spin weight (or even ill defined spin weight). Unfortunately, because of the differential behavior of $-\hat{r}$, this produces a field with the opposite spin. Thus, a more convenient operator is \bar{A} , which also conjugates the field. For the special case of operations on h , it is clear that $\bar{A} = P_-$:

$$\bar{A}\{h\} = P_-\{h\}. \quad (\text{C6})$$

However, we regard this relation as mere coincidence, and consider \bar{A} to be the more interesting operator in general.

It is convenient to find simple expressions for the behavior of modes under each of our five transformations. The main task is to find expressions for the SWSHs under evaluation at the various conjugated points. This is easily done for $s = -2$ by inspection of the functions:

$${}_s Y_{\ell,m}(P_x\hat{r}) = (-1)^m {}_s \bar{Y}_{\ell,m}(\hat{r}), \quad (\text{C7a})$$

$${}_s Y_{\ell,m}(P_y\hat{r}) = {}_s \bar{Y}_{\ell,m}(\hat{r}), \quad (\text{C7b})$$

$${}_s Y_{\ell,m}(P_z\hat{r}) = (-1)^{\ell+s} {}_s \bar{Y}_{\ell,-m}(\hat{r}), \quad (\text{C7c})$$

$${}_s Y_{\ell,m}(-\hat{r}) = (-1)^{\ell+s+m} {}_s \bar{Y}_{\ell,-m}(\hat{r}). \quad (\text{C7d})$$

Now, for example, we can write

$$P_z\{h\}(\hat{r}) = \bar{h}(P_z\hat{r}) \quad (\text{C8a})$$

$$= \sum_{\ell,m} \bar{h}^{\ell,m} {}_{-2} \bar{Y}_{\ell,m}(P_z\hat{r}) \quad (\text{C8b})$$

$$= \sum_{\ell,m} \bar{h}^{\ell,m} (-1)^\ell {}_{-2} Y_{\ell,-m}(\hat{r}) \quad (\text{C8c})$$

$$= \sum_{\ell,m} (-1)^\ell \bar{h}^{\ell,-m} {}_{-2} Y_{\ell,m}(\hat{r}) \quad (\text{C8d})$$

$$= \sum_{\ell,m} P_z\{h\}^{\ell,m} {}_{-2} Y_{\ell,m}(\hat{r}), \quad (\text{C8e})$$

where the modes of the parity-conjugate field are related to the original modes by

$$P_z\{h\}^{\ell,m} = (-1)^\ell \bar{h}^{\ell,-m}. \quad (\text{C9})$$

Finally, we can see that Eq. (3) is really the statement that the modes are invariant under reflection across the x - y plane. That is, Eq. (3) is just the statement $P_x\{h\}^{\ell,m} = h^{\ell,m}$, which is itself a specific example of the fact that nonprecessing systems themselves are invariant under that reflection.

For completeness, we now list the transformation laws for the modes under each of the operations (which we note are only valid for fields of spin weight $s = -2$).

$$P_x\{h\}^{\ell,m} = (-1)^m \bar{h}^{\ell,m}, \quad (\text{C10a})$$

$$P_y\{h\}^{\ell,m} = \bar{h}^{\ell,m}, \quad (\text{C10b})$$

$$P_z\{h\}^{\ell,m} = (-1)^\ell \bar{h}^{\ell,-m}, \quad (\text{C10c})$$

$$P_-\{h\}^{\ell,m} = \bar{A}\{h\}^{\ell,m} = (-1)^{\ell+m} \bar{h}^{\ell,-m}. \quad (\text{C10d})$$

The details of these equations are important. In particular, they show that P_x , P_y , and P_z do not behave well under rotation;

rotation of the parity-conjugated fields is not the same as parity conjugation of the rotated fields. This is unsurprising, because those parity operators are defined with respect to basis vectors, which are obviously not rotationally invariant; the operators do not commute with the usual angular-momentum operator \vec{L} . On

the other hand, P_- and \bar{A} do behave well under rotations. For this reason, we can define rotationally invariant quantities using, for example, $\int |h - \bar{A}\{h\}|^2 d\Omega$, whereas we need to optimize over attitude when defining similar quantities with respect to P_z , for example. We use these properties in Sec. II B.

-
- [1] The LIGO Scientific Collaboration and the Virgo Collaboration, *Class. Quant. Grav.* **27**, 173001 (2010).
- [2] V. Raymond, M. V. van der Sluys, I. Mandel, V. Kalogera, C. Röver, and N. Christensen, *Class. Quant. Grav.* **26**, 114007 (2009).
- [3] L. Pekowsky, J. Healy, D. Shoemaker, and P. Laguna, *Phys. Rev. D* **87**, 084008 (2013).
- [4] L. Pekowsky, R. O’Shaughnessy, J. Healy, and D. Shoemaker, *Phys. Rev. D* **88**, 024040 (2013).
- [5] The LIGO Scientific Collaboration and the Virgo Collaboration, *Phys. Rev. D* **88**, 062001 (2013).
- [6] F. D. Ryan, *Phys. Rev. D* **52**, R3159 (1995).
- [7] H. Spruit and E. S. Phinney, *Nature* **393**, 139 (1998).
- [8] D. Lai, D. F. Chernoff, and J. M. Cordes, *Astrophys. J.* **549**, 1111 (2001).
- [9] T. Bulik, D. Gondek-Rosinska, and K. Belczynski, *Mon. Not. Roy. Astro. Soc.* **352**, 1372 (2004).
- [10] P. Grandclément, M. Ihm, V. Kalogera, and K. Belczynski, *Phys. Rev. D* **69**, 102002 (2004).
- [11] C. Wang, D. Lai, and J. L. Han, *Astrophys. J.* **656**, 399 (2007).
- [12] K. Alvi, *Phys. Rev. D* **64**, 104020 (2001).
- [13] M. Boyle and A. H. Mroué, *Phys. Rev. D* **80**, 124045 (2009).
- [14] N. W. Taylor, M. Boyle, C. Reisswig, M. A. Scheel, T. Chu, L. E. Kidder, and B. Szilágyi, *Phys. Rev. D* **88**, 124010 (2013).
- [15] M. Boyle, *Phys. Rev. D* **87**, 104006 (2013).
- [16] M. Campanelli, C. O. Lousto, H. Nakano, and Y. Zlochower, *Phys. Rev. D* **79**, 084010 (2009).
- [17] E. T. Newman and R. Penrose, *J. Math. Phys.* **7**, 863 (1966).
- [18] J. N. Goldberg, A. J. Macfarlane, E. T. Newman, F. Rohrlich, and E. C. G. Sudarshan, *J. Math. Phys.* **8**, 2155 (1967).
- [19] P. Ajith, M. Boyle, D. A. Brown, S. Fairhurst, M. Hannam, I. Hinder, S. Husa, B. Krishnan, R. A. Mercer, F. Ohme, C. D. Ott, J. S. Read, L. Santamaría, and J. T. Whelan, “Data formats for numerical relativity,” (2011), [arXiv:0709.0093v3 \[gr-qc\]](https://arxiv.org/abs/0709.0093v3).
- [20] P. Schmidt, M. Hannam, S. Husa, and P. Ajith, *Phys. Rev. D* **84**, 024046 (2011).
- [21] R. O’Shaughnessy, B. Vaishnav, J. Healy, Z. Meeks, and D. Shoemaker, *Phys. Rev. D* **84**, 124002 (2011).
- [22] M. Boyle, R. Owen, and H. P. Pfeiffer, *Phys. Rev. D* **84**, 124011 (2011).
- [23] A. Buonanno, Y. Chen, and M. Vallisneri, *Phys. Rev. D* **67**, 104025 (2003).
- [24] L. E. Kidder, *Phys. Rev. D* **52**, 821 (1995).
- [25] J. D. Schnittman, A. Buonanno, J. R. van Meter, J. G. Baker, W. D. Boggs, J. Centrella, B. J. Kelly, and S. T. McWilliams, *Phys. Rev. D* **77**, 044031 (2008).
- [26] É. Racine, A. Buonanno, and L. E. Kidder, *Phys. Rev. D* **80**, 044010 (2009).
- [27] K. G. Arun, A. Buonanno, G. Faye, and E. Ochsner, *Phys. Rev. D* **79**, 104023 (2009), note that the 1.5 and 2.5pN spin terms in the flux and energy expressions do not account for an erratum from 2010.
- [28] A. Buonanno, G. Faye, and T. Hinderer, *Phys. Rev. D* **87**, 044009 (2013).
- [29] A. Bohé, S. Marsat, G. Faye, and L. Blanchet, *Class. Quant. Grav.* **30**, 075017 (2013).
- [30] A. H. Mroué, M. A. Scheel, B. Szilágyi, H. P. Pfeiffer, M. Boyle, D. A. Hemberger, L. E. Kidder, G. Lovelace, S. Ossokine, N. W. Taylor, A. Zenginoğlu, L. T. Buchman, T. Chu, E. Foley, M. Giesler, R. Owen, and S. A. Teukolsky, *Phys. Rev. Lett.* **111**, 241104 (2013), numerical data sets are available for download from the collaboration’s website.
- [31] H. Wahlquist, *Gen. Relativ. Gravit.* **19**, 1101 (1987).
- [32] G. M. Harry and t. L. S. Collaboration, *Class. Quant. Grav.* **27**, 084006 (2010).
- [33] D. Shoemaker, *LIGO-T0900288-v3: Advanced LIGO anticipated sensitivity curves*, Tech. Rep. (LIGO, 2010).
- [34] M. Favata, *Phys. Rev. D* **83**, 024028 (2011).
- [35] M. J. Fitchett, *Mon. Not. Roy. Astro. Soc.* **203**, 1049 (1983).
- [36] L. Blanchet, M. S. S. Qusailah, and C. M. Will, *Astrophys. J.* **635**, 508 (2005).
- [37] T. Damour and A. Gopakumar, *Phys. Rev. D* **73**, 124006 (2006).
- [38] M. Boyle, “Transformations of fields at future null infinity,” (2014), not yet published.
- [39] R. Arnowitt, S. Deser, and C. Misner, *Gen. Relativ. Gravit.* **40**, 1997 (2008).
- [40] G. B. Cook and H. P. Pfeiffer, *Phys. Rev. D* **70**, 104016 (2004).
- [41] G. Lovelace, R. Owen, H. P. Pfeiffer, and T. Chu, *Phys. Rev. D* **78**, 084017 (2008).
- [42] G. Lovelace, *Class. Quant. Grav.* **26**, 114002 (2009).
- [43] B. Garcia, G. Lovelace, L. E. Kidder, M. Boyle, S. A. Teukolsky, M. A. Scheel, and B. Szilágyi, *Phys. Rev. D* **86** (2012), [10.1103/PhysRevD.86.084054](https://arxiv.org/abs/10.1103/PhysRevD.86.084054).
- [44] C. Reisswig, N. T. Bishop, and D. Pollney, “General relativistic null-cone evolutions with a high-order scheme,” (2012), [arXiv:1208.3891 \[gr-qc\]](https://arxiv.org/abs/1208.3891).
- [45] J. Winicour, *Living Rev. Relativity* **15** (2012).
- [46] N. T. Bishop, R. Gómez, L. Lehner, M. Maharaj, and J. Winicour, *Phys. Rev. D* **56**, 6298 (1997).
- [47] R. Gómez, W. Barreto, and S. Frittelli, *Phys. Rev. D* **76** (2007), [10.1103/PhysRevD.76.124029](https://arxiv.org/abs/10.1103/PhysRevD.76.124029).
- [48] R. K. Sachs, *Phys. Rev.* **128**, 2851 (1962).
- [49] R. Geroch and J. Winicour, *J. Math. Phys.* **22**, 803 (1981).
- [50] T. Dray and M. Streubel, *Class. Quant. Grav.* **1**, 15 (1984).
- [51] O. M. Moreschi, *Class. Quant. Grav.* **3**, 503 (1986).
- [52] H. Bondi, M. G. J. v. d. Burg, and A. W. K. Metzner, *Proc. Roy. Soc. A* **269**, 21 (1962).
- [53] J. Winicour, “General relativity and gravitation,” (Plenum, New York, 1980) pp. 71–96.
- [54] M. Campanelli and C. O. Lousto, *Phys. Rev. D* **59**, 124022 (1999).
- [55] C. O. Lousto and Y. Zlochower, *Phys. Rev. D* **76**, 041502 (2007).

- [56] M. Ruiz, M. Alcubierre, D. Núñez, and R. Takahashi, *Gen. Relativ. Gravit.* **40**, 1705 (2008).
- [57] C. O. Lousto and Y. Zlochower, *Phys. Rev. D* **89**, 021501 (2014).
- [58] S. E. Gralla, A. I. Harte, and R. M. Wald, *Phys. Rev. D* **81** (2010), 10.1103/PhysRevD.81.104012.
- [59] K. S. Thorne, *Rev. Mod. Phys.* **52**, 299 (1980).
- [60] L. Blanchet, *Living Rev. Relativity* **17** (2014), 10.12942/lrr-2014-2.
- [61] L. S. Finn and D. F. Chernoff, *Phys. Rev. D* **47**, 2198 (1993).
- [62] T. A. Apostolatos, C. Cutler, G. J. Sussman, and K. S. Thorne, *Phys. Rev. D* **49**, 6274 (1994).
- [63] C. M. Will and A. G. Wiseman, *Phys. Rev. D* **54**, 4813 (1996).
- [64] L. Blanchet, G. Faye, B. R. Iyer, and S. Sinha, *Class. Quant. Grav.* **25**, 165003 (2008), note erratum.
- [65] G. Faye, S. Marsat, L. Blanchet, and B. R. Iyer, *Class. Quant. Grav.* **29**, 175004 (2012).
- [66] C. Doran and A. Lasenby, *Geometric algebra for physicists*, 3rd ed. (Cambridge University Press, 2003).
- [67] M. Boyle, L. E. Kidder, S. Ossokine, and H. P. Pfeiffer, “Constructing and analyzing gravitational waveforms from precessing black-hole binaries,” (2014), not yet published.
- [68] M. Campanelli, C. O. Lousto, Y. Zlochower, and D. Merritt, *Phys. Rev. Lett.* **98**, 231102 (2007).
- [69] M. Campanelli, C. Lousto, Y. Zlochower, and D. Merritt, *Astrophys. J. Lett.* **659**, L5 (2007).
- [70] W. Tichy and P. Marronetti, *Phys. Rev. D* **76**, 061502 (2007).
- [71] J. A. González, M. Hannam, U. Sperhake, B. Brügmann, and S. Husa, *Phys. Rev. Lett.* **98**, 231101 (2007).
- [72] B. Brügmann, J. A. González, M. Hannam, S. Husa, and U. Sperhake, *Phys. Rev. D* **77**, 124047 (2008).
- [73] C. O. Lousto and Y. Zlochower, *Phys. Rev. Lett.* **107**, 231102 (2011).
- [74] Eq. (C.7) of M. Alcubierre, *Introduction to 3+1 Numerical Relativity* (Oxford University Press, New York, 2008).
- [75] T. Frankel, *The geometry of physics: An introduction*, 2nd ed. (Cambridge Univ. Press, New York, 2004).
- [76] C. Loken, D. Gruner, L. Groer, R. Peltier, N. Bunn, M. Craig, T. Henriques, J. Dempsey, C.-H. Yu, J. Chen, L. J. Dursi, J. Chong, S. Northrup, J. Pinto, N. Knecht, and R. V. Zon, *J. Phys.: Conf. Ser.* **256**, 012026 (2010).
- [77] P. Ajith *et al.*, *Class. Quant. Grav.* **29**, 124001 (2012).
- [78] K. M. Huffmanberger and B. D. Wandelt, *Astrophys. J. Supp. Ser.* **189**, 255 (2010).